HHS Public Access

Author manuscript

Neuron. Author manuscript; available in PMC 2018 February 08.

Published in final edited form as:

Neuron. 2017 February 08; 93(3): 574–586.e8. doi:10.1016/j.neuron.2016.12.021.

Phosphatidylserine Exposure Controls Viral Innate Immune Responses by Microglia

Yusuf Tufail[1], **Daniela Cook**[1], **Lawrence Fourgeaud**[2], **Colin J. Powers**[3], **Katharina Merten**[1], **Charles L. Clark**[1], **Elizabeth Hoffman**[1], **Alexander Ngo**[1], **Kohei J. Sekiguchi**[1], **Clodagh C. O'Shea**[3], **Greg Lemke**[2,4], and **Axel Nimmerjahn**[1,5,*]

[1]Waitt Advanced Biophotonics Center, The Salk Institute for Biological Studies, 10010 North Torrey Pines Road, La Jolla, CA 92037, USA

[2]Molecular Neurobiology Laboratory, The Salk Institute for Biological Studies, 10010 North Torrey Pines Road, La Jolla, CA 92037, USA

[3]Molecular and Cell Biology Laboratory, The Salk Institute for Biological Studies, 10010 North Torrey Pines Road, La Jolla, CA 92037, USA

[4]Immunobiology and Microbial Pathogenesis Laboratory, The Salk Institute for Biological Studies, 10010 North Torrey Pines Road, La Jolla, CA 92037, USA

SUMMARY

Microglia are the intrinsic immune sentinels of the central nervous system. Their activation restricts tissue injury and pathogen spread, but in some settings, including viral infection, this response can contribute to cell death and disease. Identifying mechanisms that control microglial responses is therefore an important objective. Using replication-incompetent adenovirus 5 (Ad5)-based vectors as a model, we investigated the mechanisms through which microglia recognize and respond to viral uptake. Transgenic, immunohistochemical, molecular-genetic, and fluorescence imaging approaches revealed that phosphatidylserine (PtdSer) exposure on the outer leaflet of transduced cells triggers their engulfment by microglia through TAM receptor-dependent mechanisms. We show that inhibition of phospholipid scramblase 1 (PLSCR1) activity reduces

*Correspondence: animmerj@salk.edu.
[5]Lead Contact

SUPPLEMENTAL INFORMATION

Supplemental Information includes seven figures and three movies and can be found with this article online at http://dx.doi.org/10.1016/j.neuron.2016.12.021.

AUTHOR CONTRIBUTIONS

Y.T. designed, conducted, and analyzed experiments described in Figures 1, 3, 4, 6, S1–S4, and S6, wrote parts of the methods section with help from C.L.C., L.F., and C.J.P., and prepared figures with help from A. Nimmerjahn, D.C., E.H., C.L.C., and K.M.; D.C. conducted and analyzed experiments in Figures 1, 2, 3, 4, 6, and S1–S7, wrote parts of the methods section, and helped with figure preparation; L.F. helped with TAM receptor immunostaining, imaging, qPCR design, and analysis; G.L. provided TAM receptor knockout mice and experimental advice; C.J.P. and C.C.O. provided the proprietary AdSyn series of Ad5 vectors and advice on vector design, genome assembly, and multiple transgene expression; C.C.O. and C.J.P. provided optimized protocols for the production, purification, and titering of Ad5-based vectors that minimize immune cell association and inflammation; K.M. analyzed data in Figures 5 and S7; C.L.C. designed and constructed all Ad5 vectors, conducted and analyzed cell culture experiments, helped with data analysis, and wrote parts of the methods section; E.H. helped with Ad5 injections, immunostaining, and confocal imaging; A. Ngo helped with immunostaining and data analysis; K.J.S. helped with data analysis and movie preparation; A. Nimmerjahn designed the study with input from G.L., Y.T., C.L.C., and C.J.P., performed experiments in Figures 2, 5, S5, and S7 and Movies S1, S2, and S3, prepared figures and movies, and wrote the manuscript; all authors edited or reviewed the manuscript.

intracellular calcium dysregulation, prevents PtdSer externalization, and enables months-long protection of vector-transduced, transgene-expressing cells from microglial phagocytosis. Our study identifies PLSCR1 as a potent target through which the innate immune response to viral vectors, and potentially other stimuli, may be controlled.

INTRODUCTION

Microglia are the first responders to central nervous system (CNS) injury or disease (Ransohoff and Perry, 2009). As innate immune sensors, these cells are equipped with a suite of receptors that allow them to detect disturbances in their microenvironment through the presence or absence of soluble and membrane-bound signals whose expression may be triggered by intrinsic or extrinsic events (Kettenmann et al., 2011; Tremblay et al., 2011). Microglia activation leads to an inflammatory response typically aimed at restricting tissue injury or pathogen spread. Under certain conditions, maladaptive innate immune responses can lead to undesired cell loss through microglial phagocytosis (Brown and Neher, 2014).

A key, so-called “eat-me” signal for phagocytosis is phosphatidylserine (PtdSer) (Arandjelovic and Ravichandran, 2015; Lemke, 2013; Sierra et al., 2013). PtdSer is a phospholipid constituent of all eukaryotic cell membranes but displays a remarkable asymmetry in its distribution in that it is normally confined to the inner (cytoplasm-facing) leaflet of the plasma membrane. During apoptosis or cell stress, PtdSer is externalized, potentially serving as a tag for engulfment of these cells by microglia and other professional phagocytes (Arandjelovic and Ravichandran, 2015; Brown and Neher, 2014; Sierra et al., 2013). Microglia can detect tagged cells, for example, through contact-mediated sensing enabled by continual extension and retraction of microglial cell processes (Davalos et al., 2005; Fourgeaud et al., 2016; Nimmerjahn et al., 2005). PtdSer orientation in the plasma membrane is regulated by calcium-dependent and -independent phospholipid transporters (Frey and Gaipl, 2011). High intracellular calcium concentrations are thought to promote PtdSer externalization (Segawa and Nagata, 2015). However, the circumstances that lead to intracellular calcium dysregulation, PtdSer externalization, and microglia activation in vivo are, for the most part, unknown.

Viral infections of the CNS trigger innate immune responses that can include microglia phagocytosis (Sierra et al., 2013; Swanson and McGavern, 2015; Vasek et al., 2016). In particular, adenovirus (Ad)-based expression vectors are important reagents for gene transfer in the CNS. Ad5-based vectors are one of the most widely used vectors in both basic research applications and gene therapy. They are particularly attractive agents in the CNS, where cellular division is limited, which, in principle, would enable long-term transgene expression. However, previous studies have reported that Ad5-based vectors can induce potent inflammatory responses and undesired cell loss to which microglia are thought to contribute (Castro et al., 2014; Hendrickx et al., 2014; Tobias et al., 2013; Wold and Toth, 2013). The underlying effector mechanisms remain poorly understood.

In this study, using intracranial delivery of replication-incompetent, Ad5-based vectors as a model, we sought to identify signaling pathways through which microglia recognize and respond to viral uptake and to define target mechanisms for the modulation of innate

immune responses. We demonstrate that Ad5 delivery leads to dysregulation of intracellular calcium homeostasis and PtdSer externalization on the plasma membrane of transduced cells. We identify microglial TAM receptors and their ligands as key agents required for phagocytosis of PtdSer-tagged cells and phospholipid scramblase 1 (PLSCR1) activity as an effective target for the control of intracellular calcium homeostasis, PtdSer externalization, and microglia phagocytosis. Importantly, cells rescued from engulfment by microglia through PLSCR1 inhibition remained viable, resulting in prolonged transgene expression from Ad5 vectors. Together, our study identifies key molecular mechanisms mediating the interaction between Ad vector-transduced cells and innate immune sensors, which may be exploited for the construction of safer and more efficient Ad5-based vectors for both research and gene therapy applications. Given the central and conserved role of PLSCR1 in signal transduction, our findings may be relevant to other inflammatory conditions associated with intracellular calcium dysregulation, PtdSer externalization, and microglia/macrophage phagocytosis in the CNS or the periphery.

RESULTS

Microglia Engulf Adenoviral Vector-Transduced Cells

To analyze the spatiotemporal interaction of microglia with Ad5-transduced cells, we intracranially delivered a custom Ad5 vector expressing either the red fluorescent protein tdTomato (Figure 1A) or no transgene (Figure S1A and S1B) under control of the cytomegalovirus (CMV) promoter in wild-type or transgenic mice. Microglia showed markedly elevated expression of ionized calcium-binding adaptor Iba-1 and eGFP density in $Cx3cr1^{+/eGFP}$ mice, which express eGFP in microglia (Jung et al., 2000), near central regions of the transduced area. In this central area, loss of tdTomato transgene expression was observed at 3, 7, 17, and 30 days after vector injection (Figures 1A–1C, 1E, and 1F). In contrast, expression of glial fibrillary acidic protein (GFAP) was preferentially elevated at the boundary surrounding the transduced area (Figures 1B and 1D). No such Iba-1 or GFAP activation pattern was seen in vehicle controls (Figure S1C and S1D), indicating that activation was associated with viral uptake and not with injection alone. While GFAP expression around the transduced region progressively decreased over time, Iba-1 levels increased or remained elevated (Figure 1D). tdTomato-positive material within eGFP-positive cells in $Cx3cr1^{+/eGFP}$ mice indicated clearance of Ad5-transduced cells through microglial phagocytosis (Figure 1E). Microglia phagocytosis of Ad5-transduced cells was confirmed by two-photon imaging in live $Cx3cr1^{+/eGFP}$ mice (Movie S1). Consistent with this data, microglia showed an increase in the lysosomal marker CD68 in central regions (Figure 1F; Figure S1E and S1F).

Microglia-Mediated Cell Clearance Depends on Soluble and Membrane-Bound Factors

Given the chemotactic ability and process dynamics of microglia (Davalos et al., 2005; Fourgeaud et al., 2016; Nimmerjahn et al., 2005), we hypothesized that both soluble and membrane-bound factors contribute to innate immune recognition of Ad vector-transduced cells by microglia. As a first step in testing this hypothesis, we performed Ad5 vector injection in a series of mutant mice. We found that in vivo transduction leads to release of cytokines triggered, at least in part, by viral particle sensing during cell entry or intracellular

trafficking, as indicated by reduced loss of tdTomato transgene expression in Toll-like receptor (TLR) knockout and stimulator of interferon genes (STING) mutant mice (Figure S2A and S2B). Tumor necrosis factor (TNF) signaling played a particularly important role in cell clearance compared to other cytokines, such as interleukin-1 (IL-1), as demonstrated in TNF and IL-1 receptor 1 knockout mice (Figure S3A and S3B). Notably, type I interferon signaling did not significantly contribute to cell clearance despite its effect on GFAP levels (Figure S3A and S3B).

Next, we asked which membrane-bound factors and receptors mediate microglia engulfment of Ad5 vector-transduced cells. Cell clearance requires display of an eat-me signal, such as PtdSer. To determine whether PtdSer externalization might contribute to clearance of Ad5-transduced cells, we conducted experiments in live mice. Using a fixable polarity-sensitive indicator of cell viability and apoptosis (pSIVA), an Annexin B12 derivative that is membrane impermeable and emits green fluorescence only upon reversible binding to exposed PtdSer on the external plasma membrane (Kim et al., 2010; Ruggiero et al., 2012), we demonstrated an increase in pSIVA-positive cells within the transduced region at 3 days after vector injection (Figure 2A and 2B). Near central regions, punctate staining predominated, indicating cell fragmentation due to cell death or phagocytosis (Movie S1). In surrounding regions, membrane staining of morphologically intact cells was observed, suggesting the presence of stressed, but live, cells (Figure 2A).

Externalized PtdSer can be recognized by a variety of receptors (Arandjelovic and Ravichandran, 2015; Sierra et al., 2013). TAM receptor tyrosine kinases are known to mediate the phagocytosis of apoptotic cells and to regulate innate immune responses in professional phagocytes (Lemke, 2013; Rothlin et al., 2007; Zagorska et al., 2014). TAM receptor activation is dependent on PtdSer exposure in the outer leaflet of apoptotic cells, since TAM ligands bind PtdSer and bridge this phospholipid to TAM receptors (Lemke, 2013). While all TAM receptors (*Tyro3*, *Axl*, and *Mertk*) are expressed in the adult CNS, *Axl* and *Mertk* are present in microglia (Fourgeaud et al., 2016; Grommes et al., 2008). Using immunostaining, we found pronounced upregulation of *Mertk* and *Axl* in microglia near the cell clearance area at 3 days after vector injection (Figure 2C and 2D). Cell clearance was markedly reduced in $Mertk^{-/-}$ single or $Axl^{-/-}Mertk^{-/-}$ double knockout mice (Figures 3A and 3B). While $Axl^{-/-}$ $Mertk^{-/-}$ double knockout mice showed increased Iba-1 expression levels, indicating an activated microglia phenotype, GFAP expression in astrocytes around the transduced area was reduced (Figure 3A and 3B).

Modulating PLSCR1 Activity Controls Innate Immune Responses by Microglia

To further test PtdSer's involvement in cell clearance, we sought to inhibit its externalization specifically in Ad5-transduced cells. Transmembrane movement of PtdSer across the plasma membrane's lipid bilayer is regulated by phospholipid transporters, particularly calcium-dependent scramblase(s) and ATP-dependent flippase(s)/translocase(s) (Frey and Gaipl, 2011; Segawa and Nagata, 2015). Because viral infection may affect intracellular calcium signaling (Chami et al., 2006), we reasoned that altered scramblase activity due to dysregulated calcium homeostasis might contribute to increased PtdSer externalization (Zhao et al., 1998).

PLSCR is a conserved family of five genes (PLSCR1–PLSCR5) of which PLSCR1, PLSCR3, and PLSCR4 are expressed in the cortex (Zhang et al., 2014). PLSCR1, PLSCR3, and PLSCR4 possess a conserved calcium ion binding domain and a putative transmembrane region. In addition, PLSCR1 contains a nuclear localization signal and a DNA-binding domain and is upregulated in response to cytokines and other inflammatory stimuli (Kodigepalli et al., 2015). Its name notwithstanding, PLSCR1 is unlikely to possess intrinsic scramblase activity (Segawa and Nagata, 2015) but has been implicated in calcium-dependent PtdSer externalization (Zhao et al., 1998), inositol 1,4,5-triphosphate receptor (IP3R) regulation (Zhou et al., 2005), and antiviral responses in vitro (Dong et al., 2004; Yang et al., 2012). We therefore sought to inhibit its activity in vivo. We started by identifying a small hairpin RNA (shRNA) that provided specific and efficient knockdown of mouse PLSCR1 in vitro (Figure S4A). Next, we constructed two Ad5 vectors driving tdTomato expression under control of the CMV promoter, one containing the miR30-based PLSCR1-shRNA and the other incorporating a non-silencing control (NSC) shRNA (Figure 4A–4D). Remarkably, Ad5-mediated expression of PLSCR1-shRNA led to a nearly complete abrogation of microglia-mediated cell clearance in vivo (Figures 4A-4C; Figure S4B–S4H). Additionally, it significantly reduced Iba-1, GFAP, and CD68 expression levels (Figures 4D–4F; Figures S4I, S5A, and S5B). Likewise, pSIVA and microglial TAM receptor levels were significantly reduced (Figures 4G and 4H; Figures S5C–S5F). Tissue cytokine levels were also reduced (Figure 4I).

We asked whether a similar effect could be achieved by expression of calcium-insensitive $PLSCR1_{D284A}$, thought to act as a dominant-negative mutant (Ory et al., 2013). We found that this protein again abrogated cell clearance but had little effect on Iba-1 or GFAP expression levels (Figure S6A–S6D).

PLSCR1 Modulation Promotes Normal Calcium Signaling and Long-Term Protection from Microglia-Mediated Cell Clearance

Given the broadly protective effects of PLSCR1-shRNA on innate immune responses, we investigated the viability and function of Ad5 vector-transduced cells more closely.

To assess functional aspects, we performed two-photon calcium imaging in behaving mice (Mukamel et al., 2009; Nimmerjahn et al., 2009). Because most transduced and cleared cells were astrocytes (Figures S4B–S4F), we generated mice expressing the genetically encoded calcium indicator GCaMP5G under control of the GFAP promoter (Garcia et al., 2004; Gee et al., 2014). 17 days after Ad5-CMV-tdTomato-NSC-shRNA vector delivery, calcium imaging in the cortex of awake, head-restrained mice on an exercise ball revealed pronounced reduction of evoked calcium transients in NSC virus-transduced, compared to untransduced, GCaMP5G-expressing cells from the same animal (Figures 5A–5C). In contrast, mice injected with either Ad5-CMV-tdTomato-PLSCR1-shRNA or Ad5-CMV-tdTomato-$PLSCR1_{D284A}$ showed evoked calcium transients similar to those in untransduced cells from the same animal (Figures 5D–5F; Figure S7A–S7C). Closer analysis of this data revealed that calcium transient amplitude and cellular responsiveness to running onset was impaired throughout the NSC-shRNA transduced region, particularly near cell clearance regions (Figures 5G and 5H). In contrast, PLSCR1-shRNA- or $PLSCR1_{D284A}$-expressing

cells showed significantly less impaired or normal calcium transients in all transduced areas (Figures 5G and 5H; Figure S7D and S7E). Additionally, we found that NSC-shRNA-expressing cells had an increased calcium baseline (Figure 5I). In contrast, PLSCR1-shRNA- or $PLSCR1_{D284A}$-expressing cells' calcium baseline was significantly less increased (Figure 5I; Figure S7F). The observed changes in intracellular calcium signaling appeared independent of tdTomato expression levels (Figure 5J; Figures S7G) and were unlikely due to regional differences in calcium signaling (Figures S7H–S7J).

To assess long-time viability of Ad5-transduced cells, we evaluated transgene expression over several months in mice injected with either Ad5-CMV-tdTomato-NSC-shRNA or Ad5-CMV-tdTomato-PLSCR1-shRNA. We found that cell clearance, Iba-1, and GFAP levels remained low for at least 6 months after Ad5 injection when PLSCR1 activity was inhibited (Figures 6A and 6B). The vast majority of Ad5 vector-transduced, tdTomato-expressing cells, most of which were astrocytes (Figure 6A; Figure S4B and S4E), showed no overt signs of reactive morphological changes, such as thickening, blebbing, or polarization of their processes (Figures 6A).

Together, these data indicate that Ad5-transduced cells with inhibited PLSCR1 activity are protected from engulfment by microglia and persist as viable, functional transformants for weeks to months.

DISCUSSION

We demonstrate that inhibiting PLSCR1 activity and PtdSer externalization can potently inhibit microglial responses to Ad5 vector transduction without overt adverse consequences on the morphology, calcium excitability, or long-term viability of transduced cells (Figures 4, 5, and 6; Figures S6 and S7). Our data are consistent with a model (Figure 7) in which transduced cells sense viral particles during entry or intracellular trafficking, a process that likely involves TLR signaling (Figures S2A and S2B). Viral particle sensing results in an initial burst of pro-inflammatory cytokines and modulates PLSCR1 activity. The latter may be induced downstream of interferon regulatory factor 3 (IRF3), activated by calcium release and/or through an independent mechanism triggered upon viral uptake (Anand and Tikoo, 2013; Dong et al., 2004; Kodigepalli and Nanjundan, 2015; Lu et al., 2007). Activated PLSCR1 can translocate into the nucleus, for example, to enhance IP3R expression, thereby influencing intracellular calcium homeostasis (Ben-Efraim et al., 2004; Zhou et al., 2005). Dysregulated calcium signaling, mediated by IP3Rs or membrane channels (Chami et al., 2006; Khakh and McCarthy, 2015), activates plasma membrane scramblase(s). This, in turn, increases PtdSer exposure on the external surface of the plasma membrane (Figures 2A and 2B) (Frey and Gaipl, 2011; Segawa and Nagata, 2015). Note that it is unlikely that PLSCR1 promotes phospholipid scrambling at the plasma membrane directly, as phospholipid scramblase activity is unaffected in PLSCR1-deficient cells or in *Drosophila*, in which all PLSCR homologs are deleted (Kodigepalli et al., 2015; Segawa and Nagata, 2015). PtdSer exposure then allows microglia to recognize stressed Ad5 vector-transduced cells, initiate changes in TAM receptor expression and activity (Figures 2C, 2D, and 4H), and, finally, engulf the transduced, but still living, cells (Figure 3; Movie S1). Additionally, stressed cells may release damage-associated molecular patterns (DAMPs), such as ATP or high-mobility

group box 1 (HMGB1), which can be recognized by microglia (Sierra et al., 2013). Engulfment of transduced cells allows microglia to detect cellular DNA, for example, through cyclic guanine adenine synthase (cGAS)/STING or TLR9, resulting in the release of additional cytokines (Figures S2 and S3). Notably, type I IFN signaling, which is responsible for nearly all innate immune activity after lymphocytic choriomeningitis virus (LCMV) infection (Nayak et al., 2013), plays only a minor role in Ad5 transduction (Figure S3), suggesting potential involvement of a STING-dependent, but largely IFN-independent, pathway (Hasan et al., 2013). Microglia engulfment of stressed cells commences near central regions of Ad5 transduction, where multiply transduced and highly stressed cells reside and cytokine or DAMP gradients are likely highest. These gradients may serve to attract microglia (Movie S2) or stimulate their proliferation (Movie S3) (Neniskyte et al., 2014), providing a potential explanation for the increased microglia density near central regions (Figure 1B; Figure S4I).

Microglial engulfment of transduced cells can be prevented by loss of TAM receptors (Figures 3A and 3B) or by inhibiting PLSCR1 activity (Figures 4A–4D; Figure S6A and S6B). Inhibiting PLSCR1 activity, through knockdown or expression of dominant-negative calcium-insensitive PLSCR1, reduces dysregulation of intracellular calcium homeostasis (Figure 5; Figure S7) and PtdSer exposure (Figure 4G; Figure S6D) and, as a result, contact-mediated TAM receptor signaling (Figure 4H). Additionally, inhibited PLSCR1 activity results in reduced TNF-α and IL-1β expression (Figure 4I). Reduced cytokine or DAMP levels may limit microglia proliferation, phagocytosis, or their attraction to central regions (Figure 4B; Figure S4I) (Neher et al., 2014; Neniskyte et al., 2014). Reduced PtdSer exposure and TAM receptor signaling promote long-term survival of transduced cells (Figures 4G, 4H, and 6).

While we cannot rule out that an increased presence of other eat-me signals or loss of “don’t eat-me” signals might also contribute to clearance of Ad5-transduced cells, PtdSer appears to play a dominant role. Nevertheless, the fact that $Axl^{-/-}Mertk^{-/-}$ double knockout mice showed strongly reduced, but not abolished, cell clearance indicates that phagocytosis may involve additional receptor pathways (Arandjelovic and Ravichandran, 2015; Fricker et al., 2012). Likewise, while microglia are key players in phagocytic removal of stressed or apoptotic cells, other resident or non-resident cells may also contribute to cell clearance (Chung et al., 2013; Elmore et al., 2014). While our data do not support a major role of astrocytes in cell clearance (Figures 1B, 1D, 1F, 2C, and 2D; Figure S4B and S4D; Movies S1 and S2), use of high vector doses ($\geq 10^8$ IU) or prior immunization has been shown to recruit CD8+ T cells to the intracranial vector injection site (Zirger et al., 2006, 2012).

PLSCR1 activity modulation in Ad5 vector-transduced cells was broadly protective to both transgene-expressing and surrounding cells (Figures 4, 5, and 6; Figures S4, S6, and S7), suggesting that this perturbation exerts protective effects beyond intracellular calcium and PtdSer regulation. Diminished reactive changes in and loss of transduced astrocytes, an important regulatory cell type in the CNS, likely contribute to maintained tissue homeostasis, reduced secondary cell damage/loss (Figure S4E and S4F), or blood-brain barrier integrity (Obermeier et al., 2013). We also noticed a reduction in tdTomato levels in PLSCR1-shRNA- and $PLSCR1_{D284A}$-transduced, compared to NSC-vector-transduced, cells

(Figure 5J; Figure S7G). While this effect may contribute to reduced cell stress, microglia activation was comparable in Ad5-CMV Null-transduced mice (Figure S1A and S1B).

The strong effect of PLSCR1 modulation on cell clearance and immunoreactivity argues for a role of this protein upstream of TLR9 and STING, which are highly expressed on cortical microglia, but not astrocytes (Zhang et al., 2016). In contrast, the strong effect of TNF knockout on cell clearance and immunoreactivity indicates its potential role in initiating PLSCR1 activity changes. To further define the sequential engagement of these signaling pathways in Ad5-mediated innate immune responses, it will be necessary to knock out one or multiple Toll-like, cytokine, or other receptor pathways in a cell-type-specific manner.

Our experiments suggest that, by reducing the levels of chemotactic cues and externalized PtdSer, vector-transduced cells can escape microglia detection and phagocytosis. This approach therefore holds promise for constructing Ad-based vectors with reduced inflammatory responses and cell loss, potentially allowing prolonged expression of therapeutic genes in preclinical and clinical gene therapy trials (Castro et al., 2014; Soria et al., 2010; Tobias et al., 2013; Wold and Toth, 2013). In vitro studies indicate that PLSCR1 may also play important roles in the antiviral response to other viruses, including herpes simplex virus (Talukder et al., 2012), vesicular stomatitis virus (Dong et al., 2004), and hepatitis B and C viruses (Metz et al., 2012; Yuan et al., 2015). Beyond virus infection, PLSCR1 may be of importance in bacterial infection (Goth and Stephens, 2001; Lu et al., 2007), autoimmune disease (Amengual et al., 2013; Bernales et al., 2008; Suzuki et al., 2010), or cancer development (Fan et al., 2012; Kodigepalli et al., 2013; Kuo et al., 2011). However, because the pathways involved in PLSCR1 activity modulation may differ between cell types and tissues (Lu et al., 2007), further studies are needed to determine how PLSCR1 knockdown or $PLSCR1_{D284A}$ expression may benefit these conditions. This notwithstanding, all of these findings suggest that our approach may be applicable to a variety of inflammatory conditions in multiple disease settings.

STAR*METHODS

Detailed methods are provided in the online version of this paper and include the following:

- KEY RESOURCES TABLE
- CONTACT FOR REAGENT AND RESOURCE SHARING
- EXPERIMENTAL MODEL AND SUBJECT DETAILS
- METHOD DETAILS
  - Stereotactic Injections
  - Immunofluorescence
  - Cortical Cultures
  - Live Animal Preparation
  - Fluorescence Imaging
  - Molecular Cloning

STAR*METHODS

CONTACT FOR REAGENT AND RESOURCE SHARING

Further information and requests for reagents may be directed to, and will be fulfilled by, the Lead Contact, Axel Nimmerjahn (animmerj@salk.edu).

EXPERIMENTAL MODEL AND SUBJECT DETAILS

All procedures were performed in accordance with the National Institutes of Health guidelines for the Care and Use of Laboratory Animals and were approved by the institutional animal care and use committee (IACUC) at the Salk Institute. Mouse strains used in this study included wild-type and mutant mice. C57BL/6J wild-type mice were obtained from The Jackson Laboratory. Genotypes and sources of the mutant mice used are listed in the Key Resources Table. Both male and female mice were used with a minimum age of 12 weeks. None of these mice were involved in previous experiments or tests. Animals were not used for experiments if they showed signs of pain or distress, as defined by IACUC guidelines. Mice were randomly assigned to the experimental groups (Ad5-CMV-NSC, -PLSCR1, -PLSCR1$_{D284A}$, Null, or vehicle control). Group sample sizes were chosen based on previous studies and/or power analysis. Age-matched littermates were used as controls where possible. Mice were typically group-housed at approximately 22°C and provided with bedding and nesting material. All animals were maintained on a 12 hr light/dark cycle and given ad libitum access to standard rodent chow and water. All cell lines were cultured in HyClone DMEM high glucose media (GE Healthcare; Cat. #SH30243.01), supplemented with 10% fetal bovine serum (Thermo Fisher Scientific; Cat#26140-079). Cells were grown at 37°C in 5% CO_2.

METHOD DETAILS

Stereotactic Injections—Thin wall glass pipettes were pulled on a Sutter Flaming/Brown puller (Model P97). Pipette tips were carefully cut at an acute angle under 10x magnification using sterile techniques. Tip diameters were typically 10–15 μm. Pipettes that did not result with sharp bevels or had larger tip diameters were discarded. Adult mice (12–14 weeks old; typically male) were anesthetized with isoflurane (4% for induction; 1%–2% during surgery). Mice were head-fixed in a computer-assisted stereotactic system with digital coordinate readout and atlas targeting (Leica Angle Two). Neocortical coordinates were AP −1.82 – (−2.0) mm, ML 0.9–1.5 mm, DV 0.2–0.5 mm or AP −0.82 mm, ML 1–2 mm, DV 0.35–0.5 mm. Body temperature was maintained at 36°C–37°C with a DC temperature controller, and ophthalmic ointment was used to prevent eyes from drying. A small amount of depilator cream (Nair) was used to thoroughly remove hair over dorsal

areas of the skull. Skin was cleaned and sterilized with 70% ethanol and betadine. A midline incision (#15 scalpel blade) was made beginning just posterior to the eyes and ending just passed the lambda suture. The scalp was then pulled open and periosteum cleaned using scalpel and #3 forceps to expose desired hemisphere for calibrating the digital atlas and coordinate marking. Once reference points (bregma and lambda) were positioned using the pipette needle and entered into the program the desired target was set on the digital atlas. The injection pipette was carefully moved to the target site (using AP and ML coordinates). Next, the craniotomy site was marked and an electrical micro-drill with a fluted bit (0.5 mm tip diameter) was used to thin a 0.5–1 mm diameter part of the bone over the target injection site. Once the bone was thin enough to gently flex, a 30G needle with attached syringe was used to carefully cut and lift a very small (0.3–0.4 mm) segment of bone. Millimeter tick marks were made on each pulled capillary needle to measure volume of virus injected into the brain. A drop of virus was carefully pipetted onto parafilm (1–2 μL) in order to draw up the desired volume for injection. Once loaded with sufficient volume, the pipette needle was slowly lowered into the brain until the target depth was reached. Manual pressure was applied using a 30 mL syringe connected by shrink tubing and virus (0.4 or 0.8 μL for NSC-/PLSCR1-shRNA/Null or $PLSCR1_{D284A}$ vectors, respectively; 5.35×10^5 PFU for all vectors) or vehicle (TMN; 0.4 μL) was slowly injected over a period of 5–10 min. Once desired injection volume was delivered, the syringe's pressure valve was locked and position maintained for approximately 10 min to allow virus to spread and to avoid backflow upon needle retraction. Mice were then sutured along the incision on the scalp, given subcutaneous Buprenex SR (0.5 mg/kg) and allowed to recover before placement in their home cage.

Immunofluorescence—Mice were euthanized in their home cage at 3, 7, 17, 30, 90, or 180 days after injection using CO_2 asphyxiation at a 20% fill rate in accordance with IACUC guidelines. Mice were then quickly transcardially perfused with 10% sucrose followed by 4% paraformaldehyde (PFA). Brain tissue was carefully extracted to maintain structural integrity and allowed to incubate in 4% PFA overnight at 8°C. Brains were then thoroughly washed on a plate shaker with 1x phosphate buffered saline (PBS) three times over approximately 1 hr.

Perfused and PBS-washed brains were sectioned at 50 μm using a Leica VT1000 S model vibratome. Immunostaining was performed on floating coronal sections using standard techniques. Primary antibodies included GFAP (1:250; Millipore Cat. #MAB3402; RRID: AB_94844) and Iba-1 (1:200; Wako Cat. #019–19741; RRID: AB_839504).

For CD68, NeuN, DAPI and Axl/Mertk receptor staining, brains were perfused as stated above. After 24 hr incubation in 4% PFA, brains were washed in 1× PBS for 10 min, repeated three times. Brains were then placed in 30% sucrose solution and left at 4°C until they sank to the bottom of the conical storage tube. Brains were then frozen in O.C.T. compound-TissueTek media (Sakura Cat. #4583) over dry ice and ethanol mix. Frozen brain blocks were sectioned using a cryostat (Leica CM1800) at 12 μm thickness and collected on glass slides. For Axl/Mertk receptor staining a citrate buffer antigen retrieval protocol was applied followed by standard staining techniques. Primary antibodies included CD68 (1:200; Bio-Rad Cat. #MCA1957; RRID: AB_322219), NeuN (1:100; Millipore Cat. #ABN78;

RRID: AB_10807945), anti-Axl (1:100; R&D Systems Cat. #AF854; RRID: AB_355663) and anti-Mertk (1:100 or 1:200; R&D Systems Cat. #AF591/RRID: AB_2098565 or eBioscience Cat. #14–5751/RRID: AB_2572885, respectively). Selected tissue was co-stained with Iba-1 for analysis of Axl/Mertk expression on microglia. Cell nuclei were stained using DAPI (1:1000; Thermo Fisher Scientific Cat. #D21490).

Secondary antibodies (1:100) included Alexa Fluor 488 goat anti-rabbit (Thermo Fisher Scientific Cat. #A-11034; RRID: AB_2576217), Alexa Fluor 633 goat anti-rat (Thermo Fisher Scientific Cat. #A-21094; RRID: AB_2535749), and Alexa Fluor 633 goat anti-mouse (Thermo Fisher Scientific Cat. #A-21052; RRID: AB_2535719).

Cortical Cultures—Culture of cortical cells enriched for astrocytes was accomplished using methods provided by Thermo Fisher Scientific (thermofisher. com; Derivation and culture of cortical astrocytes). Briefly, postnatal day 1–2 wild-type mice were sacrificed, brains removed and thoroughly cleaned of meninges. All brain areas except cortices were removed using sterile techniques under a surgical stereoscope. Dissection was done in ice cold HBSS. Cells were dissociated, filtered and plated on collagen treated T-175 tissue culture flasks (Corning, Inc.). Cells were fed every 2 days with culture medium as described in the aforementioned protocol. Once confluent, cells were trypsinized and passed onto collagen-treated 35 mm glass bottom dishes (In Vitro Scientific; Cat. #D35-20-1.5-N) or standard plastic culture 10 cm dishes. When cultures reached confluency in these vessels (after approximately 1 week), astrocyte medium containing 0.25 mM dBcAMP and 0.2 ng/mL of EGF (GIBCO; Cat. #PHG0314) was used to induce differentiation and growth, respectively. Around 7 days after treatment with astrocyte medium, cultures were used for experiments. Transduction efficiency was ≥80%.

Live Animal Preparation—Under isoflurane anesthesia, mice were head-fixed with blunt ear bars on a custom surgical bed (Thorlabs) and kept at 36°C–37°C with a DC temperature controller. Depilator cream was used to remove hair on top of the mouse's head. The scalp was thoroughly cleaned and sterilized with 70% ethanol and betadine. A portion of the scalp was surgically removed to expose frontal, parietal, and interparietal skull segments. The scalp edges were attached to the lateral sides of the skull using tissue compatible adhesive. A custom-machined aluminum or titanium head plate was then affixed to the skull with Optibond (Kerr Cat. #31514) and/or dental cement (Coltene Whaledent Cat. # H00335). Mice were given Buprenex SR (0.5 mg/kg) prior to relief from anesthesia and allowed to recover for 1–3 days before imaging or habituation.

To visualize phosphatidylserine externalization in vivo (Figures 2A and 2B; Figures S5C, S5D, and S6C) mice were anesthetized with isoflurane and an approximately 3 mm diameter craniotomy was made over the vector injection site. The dura was carefully removed to facilitate dye penetration into the cortex. 200 μL of the fixable, green fluorescent polarity sensitive indicator of viability and apoptosis (pSIVA-IANBD; Novus Biologicals Cat. #NBP2–29382) (Kim et al., 2010) was applied topically for 90 min. Following this incubation period, mice were immediately perfused for tissue sectioning and immunostaining.

For imaging experiments, mice were anesthetized with isoflurane and a 2–3 mm diameter craniotomy was made over the original vector injection site. 2% agarose solution and a coverslip was used to seal the craniotomy, as previously described (Dittgen et al., 2004).

Fluorescence Imaging

Confocal Microscopy: One-photon laser-scanning confocal microscopy was performed on a Zeiss LSM 780. Three channel tiled z stacks (typically 10–40 images for 12–50 μm brain sections; 1 μm axial spacing) were acquired to produce images (laser lines: 488 nm, 561 nm, 633 nm). Image size was 512 × 512 pixels stitched into 3 × 3 tiles (frame scanning; 1.27 μs pixel dwell time; 2× averaging). Images were taken with an Olympus 20× 0.8-NA air-matched or 63× 1.4-NA oil objective.

Two-Photon Microscopy: In vivo two-photon imaging was performed as previously described (Nimmerjahn, 2012). A Sutter Movable Objective Microscope (MOM) equipped with a pulsed femtosecond Ti:Sapphire laser (Chameleon Vision or Ultra II, Coherent) with two fluorescence detection channels (dichroic, 565DXCR (Chroma); green emission filter, FF01–494/41 (Semrock); red emission filter, ET605/70M-2P (Chroma)) and H7422-40 GaAsP photomultiplier tubes (Hamamatsu) was used for imaging. Typical excitation wavelength was 880 nm. Data were acquired using an Olympus 20× 1.0-NA or a Nikon 16× 0.8-NA water immersion objective.

Molecular Cloning—To prepare the CMV-tdTomato construct, the CMV promoter was subcloned into the plasmid pUNISHER (Montesinos et al., 2011) replacing the hSYN promoter. The tdTomato gene was then subcloned into the EcoRI site downstream of the CMV promoter. The plasmid non-silencing pGIPZ shRNA miR control vector (pGIPZ-NSC) was purchased from GE Dharmacon (Cat. #RHS4346). It contained the non-silencing control (NSC) RNA sequence 5′- AUCUCGCUUGGGCGAGAGUAAG −3′, in a 318-nt miR30 shRNA cassette. The sequence used for the mouse PLSCR1 (mPLSCR1)-shRNA was 5′- GCUGGAAUACUUAGCUCAGAUC −3′, corresponding to nt 321–342 of the mPLSCR1 ORF. The 318-nt cassette containing the shRNA was synthesized in the same context as the NSC-shRNA by Integrated DNA Technologies, Coralville, IA. Both the mPLSCR1 and NSC miR30 shRNA cassettes were then subcloned into the EcoRV site in the 3′-utr region of the pUN-CMV-tdTomato plasmid to form the constructs pUN-CMV-tdTomato-mPLSCR1-shRNA and pUN-CMV-tdTomato-NSC-shRNA.

The vector pCMV6-mPLSCR1-myc-DDK containing the myc- and DDK-tagged mPLSCR1 cDNA was purchased from OriGene, Rockville, MD. A single nucleotide substitution was introduced which changed the amino acid at position 284 from aspartic acid to alanine by inverse PCR site-directed mutagenesis. The primers used for the mutagenesis were as follows: FWD 5′- GATGCAGC CAACTTTGGGATCCAG −3′ and REV 5′- AAAGTTGGCTGCATCCGTGAAGGC −3′. The CMV mutant (or wild-type) mPLSCR1-myc-DDK cassettes were then PCR amplified and subcloned into the PmeI to BamHI sites of the pDE1/DE3-P2A-tdTomato vector, in-frame with the P2A-tdTomato cassette.

Adenovirus Production and Titering—All viruses were E1/E3 deleted and generated using the AdSyn method by sequence and ligation independent cloning (SLIC) (O'Shea and Powers, 2013). First, the entire transcription cassette from each plasmid was PCR amplified and inserted by SLIC into AdSyn Ad5 E1 module pCOE1-038 that lacks the E1A/B region (Ad5 base pairs 448–3513). Next, the entire Ad5 E1 module with transcription cassette was PCR amplified and joined by SLIC with AdSyn Ad5 macromodule pCOASMM-025 that contains the remaining Ad5 genome (base pairs 3555–35938) except for a deletion of the E3 region (Ad5 base pairs 28599–30476). The E3 region was deleted for space. No transgenes or shRNAs were inserted into the deleted E3 region. All vectors were verified by sequencing. The vectors were then transfected into 293-H cells and the resultant viruses were amplified for three rounds and purified on two successive CsCl gradients. Titers of preparations ranged between 10^8 and 10^{10} infectious units/mL (based on ELISA) and the particle-to-PFU ratios were typically ≤ 100:1 (see Key Resources Table).

All viruses described in this paper were grown and amplified on 293-H cells, but were titered on 293e4/ix cells. 293e4/ix cells were seeded into 96-well tissue-culture plates in 100 μL of complete growth media (CGM) with 2% fetal bovine serum (FBS) per well one hour prior to transduction. Each virus preparation was serially diluted 1:3 in CGM with 2% FBS seven times. For comparison, a standard human adenovirus serotype 5 viral stock was purchased from American Type Culture Collection, Manassas, VA (Cat. #VR-1516). This standard virus was diluted with CGM and 2% FBS down to 5×10^5 PFU/mL, then serially diluted 1:3 in the same medium seven times. The cells were then transduced with 100 μL per well of each serial dilution of viral preparation, standard Ad5, or CGM with 2% FBS alone (untransduced control) in triplicate. Transduced cells were incubated at 37° C and 5% CO_2 for 48 hr.

Following the incubation, the inoculum was removed and the cells were fixed with 200 μL per well of an ice-cold 95% ethanol with 5% glacial acetic acid solution at −20°C for 15 min. The fixative was then removed and the wells were washed with PBS. After removing the PBS wash, 100 μL of SuperBlock Reagent (Thermo Fisher Scientific Cat. #37515) was added per well. The fixed cells were blocked at 4°C overnight.

For ELISA, the anti-adenovirus serotype 5 antibody (Abcam; Cat. #ab6982; RRID: AB_305685) was diluted 1:2000 in BupH Phosphate Buffered Saline (Thermo Fisher Scientific Cat. #28372) supplemented with 1.5% Normal Goat Serum (NGS, Jackson Labs). The SuperBlock was then decanted from each well and replaced with 75 μL per well of the diluted primary antibody. Plates were incubated in the primary antibody for 1 hr at room temperature with gentle rocking. The primary antibody was then decanted and the cells washed three times with ELISA wash buffer (20 mM Tris pH 7.5 with 150 mM NaCl and 0.1% Tween-20).

The secondary antibody, HRP conjugated goat anti-rabbit IgG (Thermo Fisher Scientific; Cat. #31460; RRID: AB_228341) was diluted 1:1000 in BupH buffer with 1.5% NGS. The cells were incubated with 75 μl of secondary antibody per well for 1 hr at room temperature with gentle rocking. The cells were then washed again three times with ELISA wash buffer. Following the last wash, the buffer was decanted and replaced with 100 μL of Detection

Reagent per well (1X PNPP [Thermo Fisher Scientific Cat. #34047] with 1X diethanolamine [Thermo Fisher Scientific Cat. #34064]). The cells were then incubated in the Detection Reagent for 10 min at room temperature in the dark. The ELISA was read on a Bio-Rad Model 680 Microplate reader using a 405 nM filter. Results were calculated from a standard curve prepared using the standard Ad5 readings.

Quantitative RT-PCR—Astrocyte-enriched cortical cultures were transduced with adenovirus constructs (MOI 20). 48 hr post-transduction, RNA was extracted according to the manufacturer's specifications (RNAeasy, QIAGEN Cat. #74104 or #75142), and then reverse transcribed using an RT Transcriptor First Strand cDNA synthesis kit (Roche; Cat. #04379012001). qRT-PCR was performed (for primers see Key Resources Table) on an Applied Biosystems 7900HT fast real-time PCR system using a 96- or 384-well plate format with 2× SYBR Green PCR master mix (Thermo Fisher Scientific Cat. #4344463). Data were processed and analyzed using cloud-based software (Applied Biosystems qPCR analysis modules; Thermo Fisher Scientific).

For ex vivo brain tissue qRT-PCR experiments, 3 or 17 days after intracranial injection of Ad5, mice were CO_2 asphyxiated and quickly perfused with 1X PBS. Whole brains were carefully removed and surgically dissected in ice cold ACSF. Cortical tissue punches were made by using a sterile 2.0 mm inner diameter round glass capillary connected with flexible shrink tubing to a 10 mL syringe. The open end of the capillary was gently pressed onto the site of vector injection and depressed to collect approximately 1.2 mm thickness of tissue. Tissue punches were then quickly pressure ejected into sterile 1.5 mL Eppendorf tubes using the connected syringe. Tubes with tissue samples were then dropped into liquid nitrogen and stored at −80°C until processed for RNA extraction, as described above.

QUANTIFICATION AND STATISTICAL ANALYSIS

Image Analysis—Mice stereotactically injected with Ad5-CMV-tdTomato-NSC-shRNA, Ad5-CMV-tdTomato-PLSCR1-shRNA or Ad5-CMV-PLSCR1 $_{D284A}$-P2A-tdTomato that showed little or no tdTomato expression at the injection site (e.g., due to backflow) were excluded from analysis. Likewise, animals/tissues in which surgery, perfusion, sectioning or antibody staining failed were excluded. Data were independently analyzed by up to three lab members and then averaged. Blinding was used where possible. No outliers were excluded from analysis.

Fixed Tissue Immunofluorescence: Cell clearance (Figures 1C, 3B, 4C, and 6B; Figures S2B, S3B, and S6B) was quantified as the area (in %) devoid of tdTomato-positive cell bodies over the total area of the transduced region. Corresponding Iba-1 and GFAP expression changes (Figures 1D, 3B, 4D, and 6B; Figures S1B, S1D, S2B, S3B, and S6B) were assessed by measuring the average fluorescence per area, followed by calculating the background corrected fluorescence. Data were normalized to the respective control hemisphere. More specifically, a 3-channel (Iba-1/Ad5-CMV-tdTomato/GFAP) maximum-intensity projection image (.lsm file) was opened in Fiji software and a region of interest (ROI) was drawn around the extent of the tdTomato-positive transduced area. The image channel was then switched to display the Iba-1 staining while maintaining the same ROI and

then selecting “Analyze:Measure” to display area, mean gray value and integrated density. Next, 2–3 separate smaller ROIs were made to analyze background fluorescence in the same manner. This procedure was repeated to measure the GFAP expression, but due to the expression profile extending beyond the limits of tdTomato-expressing cells, a custom-drawn ROI was made around the full field of view while avoiding GFAP expression from the white matter/corpus callosum, stained blood vessels, and the superficial pia mater. Total fluorescence was then calculated using the following equation:

$$\text{Total fluorescence} = \text{Integrated density} - (\text{ROI} \times \text{mean fluorescence of background})$$

Data from all animals within each respective experimental group were pooled and normalized to controls (untransduced hemispheres).

Changes in CD68, Mertk, Axl and pSIVA levels (Figures 4F–4H), and changes in the number of S100b-, NeuN-, DAPI-, Iba-1-, GFAP- and tdTomato-positive cells (Figure S4D, S4F, S4H, and S4I) were analyzed using Imaris (version 7 or 8; Bitplane). First, background subtraction was performed using a Gaussian filter (276 μm width) applied to each image within the three-channel tiled confocal z stacks. We then used the creation wizard feature in Imaris to generate digital representations of immunostained cells/structures, so-called “Spots” or “Surfaces.”

“Spots” were created for spherical-shaped entities such as NeuN- or DAPI-positive cell bodies (Figure S4E and S4G) and CD68-, pSIVA-, Mertk- or Axl-positive puncta (Figures 1F and 2A–2D; Figures S1E, S1F, S5A–S5F, S6C, and S6D). The following “XY Diameter” spot size filter values were used: 10 μm, 8 μm or 3 μm for NeuN-, DAPI-, or CD68 / pSIVA / Mertk- / Axl-positive structures, respectively. As “Quality” filter values we used: 1–3, 2–3, 2 or 1 for NeuN-, DAPI-, Mertk- or Axl-positive structures, respectively, depending on staining quality, to include the top 50% of spots. For CD68- and pSIVA-positive spots, the quality filter was set to include the top 1% of spots. “Quality” is the intensity value at the center of a spot in the channel the spots were detected. The same filter settings were used for corresponding control hemisphere images.

Spots were also created for quantifying the number of tdTomato-positive cell bodies (Figures 1B and 4B; S4I), using a spot size diameter of 10 μm and a quality filter to include the top 10% of spots. Non-spherical, tdTomato-positive structures such as astrocytic endfeet or polarized processes were excluded from cell counts. Dim cell bodies (e.g., near image stitching regions) were manually added to the cell counts.

“Surfaces” were created for morphologically more complex structures such as Iba-1-, GFAP- or S100b–positive cells (Figures 1B, 1E, 1F, 2C, 2D, and 4B; Figures S1E, S1F, S4B, S5A, and S5B). These surfaces captured cell bodies and their major processes. Surfaces were also created for tdTomato-positive cells during colocalization analysis (Figure 4G; Figure S6D). First, a smoothing Gaussian filter (0.83 μm width) was applied to the channel of interest. Then, surface filters were used. Surface filters included “Surface grain size,” “Diameter of the largest sphere which fits into object”, “Seed points diameter” and/or “Quality for seed points” (e.g., to determine whether a structure belongs to the same or a neighboring cell). The surface grain size was set to 1 μm or 0.5 μm for Iba-1/pSIVA or

GFAP/S100b/tdTomato-positive structures. The “Diameter of largest sphere” parameter was set to 7 μm, 5 μm or 10 μm for Iba-1, GFAP or pSIVA/S100b/tdTomato-positive structures, respectively. For the seed points diameter parameter we used 8 μm, 15 μm, 8.3 μm or 10 μm for Iba-1-, GFAP-, S100b- or pSIVA-positive structures, respectively. The seed points quality filter was set to include the top 10%, 50%, 30%, or 5% for Iba-1-, GFAP-, S100b- or pSIVA-positive structures. Finally, a “Number of voxels” filter was applied to eliminate surfaces below 25 voxels, 90 voxels or 10 voxels for Iba-1-, GFAP/S100b or pSIVA/tdTomato-positive structures.

Created spots and surfaces were then used to determine colocalization with the MATLAB function in Imaris (e.g., to quantify the levels of CD68, Mertk or Axl on Iba-1-positive cells; Figures 4F and 4H). Spots were considered colocalized with a surface if the distance between them was ≤0.5 μm.

Three analysis regions were defined (Figure 4E, Figure S4C): $r_1 \leq 100$ μm (the typical cell clearance region in Ad5-CMV-tdTomato-injected mice), 100 μm < $r_2 \leq 200$ μm (the adjacent region with generally the highest level of tdTomato expression), and 200 μm < $r_3 \leq 350$ μm from the injection center (the distal border region). These concentric regions were created manually in Imaris and then used as filters to determine the number of cells that fall within a given radial distance from the injection site. Cell counts were normalized to area/volume, taking brain slice thickness into account. To allow comparison across animals, data were normalized to control hemispheres, whenever possible (Figures 4F and 4H; Figures S4D, S4F, and S4H). Contralateral hemispheres were analyzed using the same concentric regions placed over comparable cortical areas. This analysis approach was used for our S100b, Iba-1, GFAP, tdTomato, Mertk and Axl data (Figure 4H; Figure S4D and S4I). To quantify changes in NeuN- and DAPI-positive cells, analysis regions were further narrowed. In particular, we restricted analysis to a 100 μm-wide band within the cortical layer that included the injection site. Layer 1, which contains only few cells bodies, was excluded from analysis (Figure S4E and S4G). Region-restricted analysis was also used to quantify our CD68 data. Specifically, the area along the injection needle tract was excluded from analysis. Likewise, for analysis of our pSIVA data, we excluded the top 200 μm of the cortex from analysis to avoid artifacts due to surgical preparation. In vivo pSIVA staining required creation of a cranial window and dura removal, which may cause glial cell activation. Indeed, GFAP immunoreactivity in vehicle-injected mice with a cranial window and removed dura indicated elevated GFAP levels near surface regions (<200 μm from the pia).

In Vivo Calcium Imaging: Calcium imaging in awake, head-restrained mice was performed as previously described (Mukamel et al., 2009; Nimmerjahn et al., 2009). Corresponding image datasets were analyzed using MATLAB.

To determine whether and how calcium activity differs between Ad5-transduced and untransduced cells we stereotactically injected either Ad5-CMV-tdTomato-NSC-shRNA, Ad5-CMV-tdTomato-PLSCR1-shRNA or Ad5-CMV-PLSCR1$_{D284A}$-P2A–tdTomato into transgenic mice with widespread expression of the green fluorescent, genetically encoded calcium indicator GCaMP5G. Because the majority of Ad5-transduced cells were astrocytes (Figure 6A; Figures S4B and S4E) we generated Gfap-Cre (73.12) × CAG-GCaMP5G-

IRES-tdTomato mice (see Key Resources Table). Imaging was performed 17 days after Ad5 vector delivery and following habituation of the animal to head restraint (typically 3 sessions, 30–90 min/session, 1 session/day on 3 consecutive days prior to imaging). Ad5-transduced cells were readily distinguishable from untransduced cells based on their level and pattern of tdTomato expression (Figure 5A, 5D, and 5J; Figures S7A and S7G). Calcium activity was recorded in cortical areas at or near the depth of Ad5 vector injection (typically z = 200 μm from the pia) and at different radial distances (r) from the injection site (Figure 5G; Figure S7D and S7H). At each recording site, images were typically acquired for 20 min using a 2 Hz frame rate and 512 × 512 pixel resolution (560–700 μm field of view; 50 mW average laser power at z = 125 μm) (Figures 5A–5F; Figure S7A–S7C). No signs of phototoxicity, such as a gradual increase in baseline fluorescence, lasting changes in activity rate or blebbing of recorded cells were apparent in our recordings. The same PMT settings were used for all recordings and mice.

Based on the radial tdTomato expression profile typically found in Ad5-CMV-tdTomato-injected wild-type mice (Figure 1B), three main analysis regions were defined: $r_1 < 100$ μm (the typical cell clearance region), 100 μm $< r_2 <$ 200 μm (the adjacent region with generally the highest level of tdTomato expression), and $r_3 > 200$ μm from the injection center (the distal border region) (Figure 5; Figure S7). Untransduced cells included in analysis were located in regions with little to no GFAP activation (r > 300 μm) (Figure 1B). A comparison of untransduced cells located at various distances from the injection site (r = 300–600 μm, r = 600–1,000 μm, or r > 1,000 μm) revealed no significant effect of distance on calcium transients or GCaMP baseline expression (Figure S7H–S7J).

Cells and analysis regions were computationally defined and hence no blinding was used. For each two-channel recording we first calculated the maximum intensity projection image of the fluorescence recorded in the tdTomato channel. Next, we identified parameters suitable for automated segmentation of Ad5-transduced and untransduced tdTomato-positive cells. Because Ad5-transduced cells showed consistently higher tdTomato levels compared to untransduced cells (Figure 5J; Figure S7G) we used tdTomato levels as one parameter. In particular, for segmentation of Ad5-transduced cells we used the ~95^{th} percentile of the tdTomato pixel intensity distribution recorded at the injection site. The corresponding threshold value differed between test groups (NSC, PLSCR1, $PLSCR1_{D284A}$). For Ad5-CMV-tdTomato-NSC-shRNA or -PLSCR1-shRNA transduced cells we used a threshold value of 14,000 in 16-bit unsigned grayscale images. For Ad5-CMV-$PLSCR1_{D284A}$-P2A-tdTomato transduced cells we used 8,000. For identification of untransduced cells we used the ~95^{th} percentile of the pixel intensity distribution recorded far away from the injection site (r > 300 μm). This threshold varied between 4,000 and 7,000, depending on animal (e.g., optical window quality or brain surface blood vessel pattern).

A second parameter that we used to distinguish Ad5-transduced from untransduced cells was the labeling pattern. Cellular processes/branches of transduced cells were more apparent than those of untransduced cells, likely due to the higher levels of tdTomato expression. During segmentation, this resulted in a ‘haze’ around Ad5-transduced cells, i.e., larger cell segments for transduced compared to untransduced cells. Cell segments determined using the ‘untransduced cell’ threshold that appeared 10× larger in size than the same segment

determined using the ‘transduced cell’ threshold were classified as ‘transduced’. Otherwise, they were counted as ‘untransduced’. Segments that exceeded a size of 300 μm^2, likely representing more than one cell, were re-segmented with a higher threshold. For every such iteration the threshold was increased by 2,000. Segments >30 μm^2 were retained. Re-segmentation was repeated for a maximum of 10 iterations. All areas segmented with the ‘transduced’ threshold (or higher) were considered ‘transduced’. All areas segmented with the ‘untransduced’ threshold and non-overlapping with the transduced areas were considered ‘untransduced’. The radial distance of each identified segment from the injection center was calculated as the Euclidian distance of the segments’ centroid to the injection center.

To verify that identified tdTomato-positive segments were also GCaMP-positive, we calculated the maximum intensity projection image of the fluorescence simultaneously recorded in the GCaMP channel and applied a threshold of 10,000 (corresponding to the approximately 50^{th} percentile of the pixel intensity distribution in that channel). Segments showing less than 80% overlap of tdTomato with GCaMP expression were excluded from analysis.

GCaMP fluorescence signals, F(t), were extracted from all identified segments and corresponding temporal traces were smoothed with a Gaussian filter (s.d., 0.2 s) (Figures 5A, 5B, 5D, and 5E; Figure S7A and S7B). $\Delta F(t)/F$ was calculated as (F(t) – baseline)/baseline. Cells were considered active when $\Delta F(t)/F$ crossed a threshold, defined as the 95^{th} percentile of the filtered signal distribution of the whole recording, for >4 s.

To quantify how GCaMP baseline expression differs across test groups and analysis regions (Figure 5I; Figures S7F) we generated regions of interest (ROIs) of a fixed size (10 μm × 10 μm) around the centroid of each identified segment. This served to minimize analysis biases that could arise from segmentation with different tdTomato thresholds. For each ROI the mean GCaMP intensity over time was used as a threshold to detect calcium activity on-/offset. For baseline calculation calcium activity starting 5 s prior to a detected onset and ending 5 s after a detected offset were excluded from the trace. If the remaining intervals were longer than 20 s, the corresponding GCaMP signal was temporally averaged to yield the calcium baseline. Baseline values for each ROI were normalized to the average baseline value of all untransduced cell ROIs from the same mouse. For group analysis, baseline values were averaged for each recording and analysis region.

To quantify tdTomato expression differences across test groups and analysis regions (Figure 5J; Figures S7G), we applied the ROIs defined for quantifying GCaMP baseline expression differences to the maximum intensity projection image of fluorescence detected in the tdTomato channel. Pixel intensities for each ROI were averaged and then normalized to the average tdTomato intensity of all untransduced cells from the same mouse. For group analysis, tdTomato intensities were averaged for each recording and analysis region.

Locomotor activity of head-restrained, awake mice on the spherical treadmill was recorded using an optical encoder (US Digital Cat. #E7PD-720-118). Encoder signals were acquired at 10 kHz but, for analysis, down-sampled to 20 Hz and smoothed with a Gaussian filter (s.d., 0.7 s). Running onset or offset was defined as the time point at which running speed

exceeded 10 mm/s or fell below 4 mm/s. Because astrocyte calcium transients are typically slow, lasting several seconds (Figures 5C and 5F; Figure S7C), only calcium activity evoked by running bouts that were separated by at least 40 s from a previous running bout was included in analysis. Calcium activity was classified as running-evoked if it occurred between 5 s before and 10 s after running onset. To generate the plot of average running-evoked calcium activity, shown in Figures 5C, 5F, and S7C, calcium traces were aligned to running onset. For a given recording, responsiveness of a cell to running (Figure 5H; Figures S7E and S7H) was calculated as the proportion of running bouts that evoked astrocyte calcium activity in that cell. All cell responsiveness values were then normalized to the average responsiveness of untransduced cells from the same mouse. For group analysis, responsiveness values were averaged for each recording and analysis region.

For the analysis of calcium baseline, tdTomato expression, and responsiveness to running events we used a two-way ANOVA with two fixed factors, namely test group (NSC, PLSCR1 or PLSCR1$_{D284A}$) and cell transduction state (transduced or untransduced). All three comparisons showed significant effects for both factors ($p < 0.01$). A t test was used to compare calcium baseline, tdTomato expression and responsiveness to running events of transduced cells across test groups. The NSC group showed significantly higher tdTomato expression than the PLSCR1 and PLSCR1$_{D284A}$ group ($p < 0.5$, Bonferroni corrected). To test for differences between transduced and untransduced cells within test groups, we used a paired t test. In the NSC group, the responsiveness to running events of transduced cells with 100 μm $< r_2 \leq$ 200 μm or $r_3 >$ 200 μm was significantly lower than the responsiveness of untransduced cells ($p < 0.05$, Bonferroni corrected). In the PLSCR1 group, the responsiveness of transduced cells with 100 μm $< r_2 \leq$ 200 μm or $r_3 >$ 200 μm was not significantly different compared to the responsiveness of untransduced cells ($p > 0.05$). In the PLSCR1$_{D284A}$ group, the responsiveness of transduced cells with 100 μm $< r_2 \leq$ 200 μm was significantly lower compared to the responsiveness of untransduced cells ($p < 0.05$, Bonferroni corrected). Transduced cells with $r_3 >$ 200 μm showed responsiveness comparable to that of untransduced cells ($p > 0.05$, Bonferroni corrected). We also tested whether calcium baseline level, tdTomato expression and responsiveness to running events of untransduced cells varied with distance from the injection site. We used a two-way ANOVA with a fixed factor ‘test group’ (NSC, PLSCR1 or PLSCR1$_{D284A}$) and a fixed continuous factor ‘radial distance from the injection site’ (r = 300–600 μm, 600–1,000 μm, or >1,000 μm). No significant effect was found ($p > 0.05$).

Statistical Analysis—Statistical details of experiments, including statistical test used and statistical significance, can be found in the figure legends or Method Details above with “n” denoting the number of animals per experimental group and “N” the number of brain sections analyzed per animal. Group sample sizes were chosen based on previous studies and/or power analysis. Data were processed, analyzed and plotted using MATLAB, Fiji, Excel, or Prism software. All datasets displayed normal distribution and equal standard deviations unless indicated by unequal variance test (Welch’s). Data were judged to be statistically significant when $p < 0.05$. The following convention was used to indicate p values in Figures 1, 3, 4, 5, 6, Figures S1–S4, S6, and S7: “n.s.” (not significant) indicates $p \geq 0.05$, “*” indicates $0.01 \leq p < 0.05$, “**” indicates $0.001 \leq p < 0.01$, “***” indicates

$0.0001 \leq p < 0.001$, and "****" indicates $p < 0.0001$. All data are represented as mean ± SEM.

Supplementary Material

Refer to Web version on PubMed Central for supplementary material.

Acknowledgments

We thank Edward M. Callaway and Fred H. Gage for critical feedback and advice; Joseph Chambers for mouse colony management; Jamie Simon for help with Figure 7; the Max Planck Florida Institute for the pUNISHER plasmid; the Waitt Advanced Biophotonics Center and Histology Core facilities for help with in vitro microscopy and tissue preparation, respectively; and all members of the A. Nimmerjahn lab for critical feedback; A. Nimmerjahn was supported by grants from the NIH (New Innovator Award, DP2 NS083038, and EUREKA Award, R01 NS085938 to A. Nimmerjahn; P30 CA014195 and P30 NS072031 to the Salk Institute), and funds from the Rita Allen, Whitehall, Brain Research, Waitt, Hearst, and Richard Allan Barry Family Foundations; G.L. was supported by funds from the NIH (R01 AI101400 and R01 NS085296 to G.L. and P30 CA014195 to the Salk Institute), the Leona M. and Harry B. Helmsley Charitable Trust (#2012-PG-MED002 to the Salk Institute), the Nomis, H.N. and Frances C. Berger, Fritz B. Burns, and HKT Foundations, and by Frederik Paulson and Françoise Gilot-Salk; C.C.O. was supported by funds from the NCI (R01 CA137094-06 to C.C.O., and P30 CA014195 to the Salk Institute), the Leona M. and Harry B. Helmsley Charitable Trust (#2012-PG-MED002 to the Salk Institute), the William Scandling Trust, the Price Family Foundation, and the Marshall Legacy Foundation; Y.T. is a Howard Hughes Medical Institute Fellow of the Life Sciences Research Foundation and recipient of a Pioneer Fund postdoctoral scholar award; K.M. is a DFG research fellow and recipient of a Catharina Foundation postdoctoral scholar award.

REFERENCES

Amengual O, Atsumi T, Oku K, Suzuki E, Horita T, Yasuda S, Koike T. Phospholipid scramblase 1 expression is enhanced in patients with antiphospholipid syndrome. Mod. Rheumatol. 2013; 23:81–88. [PubMed: 22526829]

Anand SK, Tikoo SK. Viruses as modulators of mitochondrial functions. Adv. Virol. 2013; 2013:738794. [PubMed: 24260034]

Arandjelovic S, Ravichandran KS. Phagocytosis of apoptotic cells in homeostasis. Nat. Immunol. 2015; 16:907–917. [PubMed: 26287597]

Ben-Efraim I, Zhou Q, Wiedmer T, Gerace L, Sims PJ. Phospholipid scramblase 1 is imported into the nucleus by a receptor-mediated pathway and interacts with DNA. Biochemistry. 2004; 43:3518–3526. [PubMed: 15035622]

Bernales I, Fullaondo A, Marín-Vidalled MJ, Ucar E, Martínez-Taboada V, López-Hoyos M, Zubiaga AM. Innate immune response gene expression profiles characterize primary antiphospholipid syndrome. Genes Immun. 2008; 9:38–46. [PubMed: 17960154]

Brown GC, Neher JJ. Microglial phagocytosis of live neurons. Nat. Rev. Neurosci. 2014; 15:209–216. [PubMed: 24646669]

Castro MG, Candolfi M, Wilson TJ, Calinescu A, Paran C, Kamran N, Koschmann C, Moreno-Ayala MA, Assi H, Lowenstein PR. Adenoviral vector-mediated gene therapy for gliomas: coming of age. Expert Opin. Biol. Ther. 2014; 14:1241–1257. [PubMed: 24773178]

Chami M, Oulés B, Paterlini-Bréchot P. Cytobiological consequences of calcium-signaling alterations induced by human viral proteins. Biochim. Biophys. Acta. 2006; 1763:1344–1362. [PubMed: 17059849]

Chung WS, Clarke LE, Wang GX, Stafford BK, Sher A, Chakraborty C, Joung J, Foo LC, Thompson A, Chen C, et al. Astrocytes mediate synapse elimination through MEGF10 and MERTK pathways. Nature. 2013; 504:394–400. [PubMed: 24270812]

Davalos D, Grutzendler J, Yang G, Kim JV, Zuo Y, Jung S, Littman DR, Dustin ML, Gan WB. ATP mediates rapid microglial response to local brain injury in vivo. Nat. Neurosci. 2005; 8:752–758. [PubMed: 15895084]

Dittgen T, Nimmerjahn A, Komai S, Licznerski P, Waters J, Margrie TW, Helmchen F, Denk W, Brecht M, Osten P. Lentivirus-based genetic manipulations of cortical neurons and their optical and electrophysiological monitoring in vivo. Proc. Natl. Acad. Sci. USA. 2004; 101:18206–18211. [PubMed: 15608064]

Dong B, Zhou Q, Zhao J, Zhou A, Harty RN, Bose S, Banerjee A, Slee R, Guenther J, Williams BR, et al. Phospholipid scramblase 1 potentiates the antiviral activity of interferon. J. Virol. 2004; 78:8983–8993. [PubMed: 15308695]

Elmore MR, Najafi AR, Koike MA, Dagher NN, Spangenberg EE, Rice RA, Kitazawa M, Matusow B, Nguyen H, West BL, Green KN. Colony-stimulating factor 1 receptor signaling is necessary for microglia viability, unmasking a microglia progenitor cell in the adult brain. Neuron. 2014; 82:380–397. [PubMed: 24742461]

Fan CW, Chen CY, Chen KT, Shen CR, Kuo YB, Chen YS, Chou YP, Wei WS, Chan EC. Blockade of phospholipid scramblase 1 with its N-terminal domain antibody reduces tumorigenesis of colorectal carcinomas in vitro and in vivo. J. Transl. Med. 2012; 10:254. [PubMed: 23259795]

Fourgeaud L, Través PG, Tufail Y, Leal-Bailey H, Lew ED, Burrola PG, Callaway P, Zagórska A, Rothlin CV, Nimmerjahn A, Lemke G. TAM receptors regulate multiple features of microglial physiology. Nature. 2016; 532:240–244. [PubMed: 27049947]

Frey B, Gaipl US. The immune functions of phosphatidylserine in membranes of dying cells and microvesicles. Semin. Immunopathol. 2011; 33:497–516. [PubMed: 20941495]

Fricker M, Neher JJ, Zhao JW, Théry C, Tolkovsky AM, Brown GC. MFG-E8 mediates primary phagocytosis of viable neurons during neuroinflammation. J. Neurosci. 2012; 32:2657–2666. [PubMed: 22357850]

Garcia AD, Doan NB, Imura T, Bush TG, Sofroniew MV. GFAP-expressing progenitors are the principal source of constitutive neuro-genesis in adult mouse forebrain. Nat. Neurosci. 2004; 7:1233–1241. [PubMed: 15494728]

Gee JM, Smith NA, Fernandez FR, Economo MN, Brunert D, Rothermel M, Morris SC, Talbot A, Palumbos S, Ichida JM, et al. Imaging activity in neurons and glia with a Polr2a–based and cre-dependent GCaMP5G–IRES-tdTomato reporter mouse. Neuron. 2014; 83:1058–1072. [PubMed: 25155958]

Goth SR, Stephens RS. Rapid, transient phosphatidylserine externalization induced in host cells by infection with Chlamydia spp. Infect. Immun. 2001; 69:1109–1119. [PubMed: 11160008]

Grommes C, Lee CY, Wilkinson BL, Jiang Q, Koenigsknecht-Talboo JL, Varnum B, Landreth GE. Regulation of microglial phagocytosis and inflammatory gene expression by Gas6 acting on the Axl/Mer family of tyrosine kinases. J. Neuroimmune Pharmacol. 2008; 3:130–140. [PubMed: 18247125]

Hasan M, Koch J, Rakheja D, Pattnaik AK, Brugarolas J, Dozmorov I, Levine B, Wakeland EK, Lee-Kirsch MA, Yan N. Trex1 regulates lysosomal biogenesis and interferon-independent activation of antiviral genes. Nat. Immunol. 2013; 14:61–71. [PubMed: 23160154]

Hendrickx R, Stichling N, Koelen J, Kuryk L, Lipiec A, Greber UF. Innate immunity to adenovirus. Hum. Gene Ther. 2014; 25:265–284. [PubMed: 24512150]

Jung S, Aliberti J, Graemmel P, Sunshine MJ, Kreutzberg GW, Sher A, Littman DR. Analysis of fractalkine receptor CX(3)CR1 function by targeted deletion and green fluorescent protein reporter gene insertion. Mol. Cell. Biol. 2000; 20:4106–4114. [PubMed: 10805752]

Kettenmann H, Hanisch UK, Noda M, Verkhratsky A. Physiology of microglia. Physiol. Rev. 2011; 91:461–553. [PubMed: 21527731]

Khakh BS, McCarthy KD. Astrocyte calcium signaling: from observations to functions and the challenges therein. Cold Spring Harb. Perspect. Biol. 2015; 7:a020404. [PubMed: 25605709]

Kim YE, Chen J, Chan JR, Langen R. Engineering a polarity-sensitive biosensor for time-lapse imaging of apoptotic processes and degeneration. Nat. Methods. 2010; 7:67–73. [PubMed: 19966809]

Kodigepalli KM, Nanjundan M. Induction of PLSCR1 in a STING/ IRF3-dependent manner upon vector transfection in ovarian epithelial cells. PLoS ONE. 2015; 10:e0117464. [PubMed: 25658875]

Kodigepalli KM, Anur P, Spellman P, Sims PJ, Nanjundan M. Phospholipid Scramblase 1, an interferon-regulated gene located at 3q23, is regulated by SnoN/SkiL in ovarian cancer cells. Mol. Cancer. 2013; 12:32. [PubMed: 23621864]

Kodigepalli KM, Bowers K, Sharp A, Nanjundan M. Roles and regulation of phospholipid scramblases. FEBS Lett. 2015; 589:3–14. [PubMed: 25479087]

Kuo YB, Chan CC, Chang CA, Fan CW, Hung RP, Hung YS, Chen KT, Yu JS, Chang YS, Chan EC. Identification of phospholipid scramblase 1 as a biomarker and determination of its prognostic value for colorectal cancer. Mol. Med. 2011; 17:41–47. [PubMed: 20927484]

Lemke G. Biology of the TAM receptors. Cold Spring Harb. Perspect. Biol. 2013; 5:a009076.

Lu B, Sims PJ, Wiedmer T, Moser AH, Shigenaga JK, Grunfeld C, Feingold KR. Expression of the phospholipid scramblase (PLSCR) gene family during the acute phase response. Biochim. Biophys. Acta. 2007; 1771:1177–1185. [PubMed: 17590392]

Metz P, Dazert E, Ruggieri A, Mazur J, Kaderali L, Kaul A, Zeuge U, Windisch MP, Trippler M, Lohmann V, et al. Identification of type I and type II interferon-induced effectors controlling hepatitis C virus replication. Hepatology. 2012; 56:2082–2093. [PubMed: 22711689]

Montesinos MS, Chen Z, Young SM Jr. pUNISHER: a high-level expression cassette for use with recombinant viral vectors for rapid and long term in vivo neuronal expression in the CNS. J. Neurophysiol. 2011; 106:3230–3244. [PubMed: 21957229]

Mukamel EA, Nimmerjahn A, Schnitzer MJ. Automated analysis of cellular signals from large-scale calcium imaging data. Neuron. 2009; 63:747–760. [PubMed: 19778505]

Nayak D, Johnson KR, Heydari S, Roth TL, Zinselmeyer BH, McGavern DB. Type I interferon programs innate myeloid dynamics and gene expression in the virally infected nervous system. PLoS Pathog. 2013; 9:e1003395. [PubMed: 23737750]

Neher JJ, Neniskyte U, Hornik T, Brown GC. Inhibition of UDP/P2Y6 purinergic signaling prevents phagocytosis of viable neurons by activated microglia in vitro and in vivo. Glia. 2014; 62:1463–1475. [PubMed: 24838858]

Neniskyte U, Vilalta A, Brown GC. Tumour necrosis factor alpha-induced neuronal loss is mediated by microglial phagocytosis. FEBS Lett. 2014; 588:2952–2956. [PubMed: 24911209]

Nimmerjahn A. Two-photon imaging of microglia in the mouse cortex in vivo. Cold Spring Harb. Protoc. 2012; 2012:594–603.

Nimmerjahn A, Kirchhoff F, Helmchen F. Resting microglial cells are highly dynamic surveillants of brain parenchyma in vivo. Science. 2005; 308:1314–1318. [PubMed: 15831717]

Nimmerjahn A, Mukamel EA, Schnitzer MJ. Motor behavior activates Bergmann glial networks. Neuron. 2009; 62:400–412. [PubMed: 19447095]

O'Shea, CC., Powers, CJ. Adenoviral assembly method. U.S. patent. US13/769,025. 2013 Sep.

Obermeier B, Daneman R, Ransohoff RM. Development, maintenance and disruption of the blood-brain barrier. Nat. Med. 2013; 19:1584–1596. [PubMed: 24309662]

Ory S, Ceridono M, Momboisse F, Houy S, Chasserot-Golaz S, Heintz D, Calco V, Haeberle´ AM, Espinoza FA, Sims PJ, et al. Phospholipid scramblase-1-induced lipid reorganization regulates compensatory endocytosis in neuroendocrine cells. J. Neurosci. 2013; 33:3545–3556. [PubMed: 23426682]

Ransohoff RM, Perry VH. Microglial physiology: unique stimuli, specialized responses. Annu. Rev. Immunol. 2009; 27:119–145. [PubMed: 19302036]

Rothlin CV, Ghosh S, Zuniga EI, Oldstone MB, Lemke G. TAM receptors are pleiotropic inhibitors of the innate immune response. Cell. 2007; 131:1124–1136. [PubMed: 18083102]

Ruggiero L, Connor MP, Chen J, Langen R, Finnemann SC. Diurnal, localized exposure of phosphatidylserine by rod outer segment tips in wild-type but not Itgb5−/− or Mfge8−/− mouse retina. Proc. Natl. Acad. Sci. USA. 2012; 109:8145–8148. [PubMed: 22566632]

Segawa K, Nagata S. An apoptotic'eat me' signal: phosphatidylserine exposure. Trends Cell Biol. 2015; 25:639–650. [PubMed: 26437594]

Sierra A, Abiega O, Shahraz A, Neumann H. Janus-faced microglia: beneficial and detrimental consequences of microglial phagocytosis. Front. Cell. Neurosci. 2013; 7:6. [PubMed: 23386811]

Soria C, Estermann FE, Espantman KC, O'Shea CC. Heterochromatin silencing of p53 target genes by a small viral protein. Nature. 2010; 466:1076–1081. [PubMed: 20740008]

Suzuki E, Amengual O, Atsumi T, Oku K, Hashimoto T, Kataoka H, Horita T, Yasuda S, Ieko M, Fukushima K, Koike T. Increased expression of phospholipid scramblase 1 in monocytes from patients with systemic lupus erythematosus. J. Rheumatol. 2010; 37:1639–1645. [PubMed: 20516018]

Swanson PA 2nd, McGavern DB. Viral diseases of the central nervous system. Curr. Opin. Virol. 2015; 11:44–54. [PubMed: 25681709]

Talukder AH, Bao M, Kim TW, Facchinetti V, Hanabuchi S, Bover L, Zal T, Liu YJ. Phospholipid scramblase 1 regulates Toll-like receptor 9-mediated type I interferon production in plasmacytoid dendritic cells. Cell Res. 2012; 22:1129–1139. [PubMed: 22453241]

Tobias A, Ahmed A, Moon KS, Lesniak MS. The art of gene therapy for glioma: a review of the challenging road to the bedside. J. Neurol. Neurosurg. Psychiatry. 2013; 84:213–222. [PubMed: 22993449]

Tremblay ME, Stevens B, Sierra A, Wake H, Bessis A, Nimmerjahn A. The role of microglia in the healthy brain. J. Neurosci. 2011; 31:16064–16069. [PubMed: 22072657]

Vasek MJ, Garber C, Dorsey D, Durrant DM, Bollman B, Soung A, Yu J, Perez-Torres C, Frouin A, Wilton DK, et al. A complement-microglial axis drives synapse loss during virus-induced memory impairment. Nature. 2016; 534:538–543. [PubMed: 27337340]

Wold WS, Toth K. Adenovirus vectors for gene therapy, vaccination and cancer gene therapy. Curr. Gene Ther. 2013; 13:421–433. [PubMed: 24279313]

Yang J, Zhu X, Liu J, Ding X, Han M, Hu W, Wang X, Zhou Z, Wang S. Inhibition of Hepatitis B virus replication by phospholipid scramblase 1 in vitro and in vivo. Antiviral Res. 2012; 94:9–17. [PubMed: 22342889]

Yuan Y, Tian C, Gong Q, Shang L, Zhang Y, Jin C, He F, Wang J. Interactome map reveals phospholipid scramblase 1 as a novel regulator of hepatitis B virus x protein. J. Proteome Res. 2015; 14:154–163. [PubMed: 25365352]

Zagorska A, Traves PG, Lew ED, Dransfield I, Lemke G. Diversification of TAM receptor tyrosine kinase function. Nat. Immunol. 2014; 15:920–928. [PubMed: 25194421]

Zhang Y, Chen K, Sloan SA, Bennett ML, Scholze AR, O'Keeffe S, Phatnani HP, Guarnieri P, Caneda C, Ruderisch N, et al. An RNA-sequencing transcriptome and splicing database of glia, neurons, and vascular cells of the cerebral cortex. J. Neurosci. 2014; 34:11929–11947. [PubMed: 25186741]

Zhang Y, Sloan SA, Clarke LE, Caneda C, Plaza CA, Blumenthal PD, Vogel H, Steinberg GK, Edwards MS, Li G, et al. Purification and characterization of progenitor and mature human astrocytes reveals transcriptional and functional differences with mouse. Neuron. 2016; 89:37–53. [PubMed: 26687838]

Zhao J, Zhou Q, Wiedmer T, Sims PJ. Level of expression of phospholipid scramblase regulates induced movement of phosphatidylserine to the cell surface. J. Biol. Chem. 1998; 273:6603–6606. [PubMed: 9506954]

Zhou Q, Ben-Efraim I, Bigcas JL, Junqueira D, Wiedmer T, Sims PJ. Phospholipid scramblase 1 binds to the promoter region of the inositol 1,4,5-triphosphate receptor type 1 gene to enhance its expression. J. Biol. Chem. 2005; 280:35062–35068. [PubMed: 16091359]

Zirger JM, Barcia C, Liu C, Puntel M, Mitchell N, Campbell I, Castro M, Lowenstein PR. Rapid upregulation of interferon-regulated and chemokine mRNAs upon injection of 10^8 international units, but not lower doses, of adenoviral vectors into the brain. J. Virol. 2006; 80:5655–5659. [PubMed: 16699048]

Zirger JM, Puntel M, Bergeron J, Wibowo M, Moridzadeh R, Bondale N, Barcia C, Kroeger KM, Liu C, Castro MG, Lowenstein PR. Immune-mediated loss of transgene expression from virally transduced brain cells is irreversible, mediated by IFNγ, perforin, and TNFα, and due to the elimination of transduced cells. Mol. Ther. 2012; 20:808–819. [PubMed: 22233583]

Highlights

- Phosphatidylserine exposure tags virally transduced cells for microglial phagocytosis
- Engulfment by microglia is TAM receptor dependent
- Inhibition of phospholipid scramblase 1 activity protects from phagocytosis
- Rescued cells remain viable allowing prolonged transgene expression

In Brief

Tufail et al. show that inhibiting phospholipid scramblase 1 activity in virally transduced cells prevents intracellular calcium dysregulation, phosphatidylserine externalization, and TAM receptor-dependent microglial phagocytosis, providing a novel mechanism through which innate immune responses to viral vectors may be controlled.

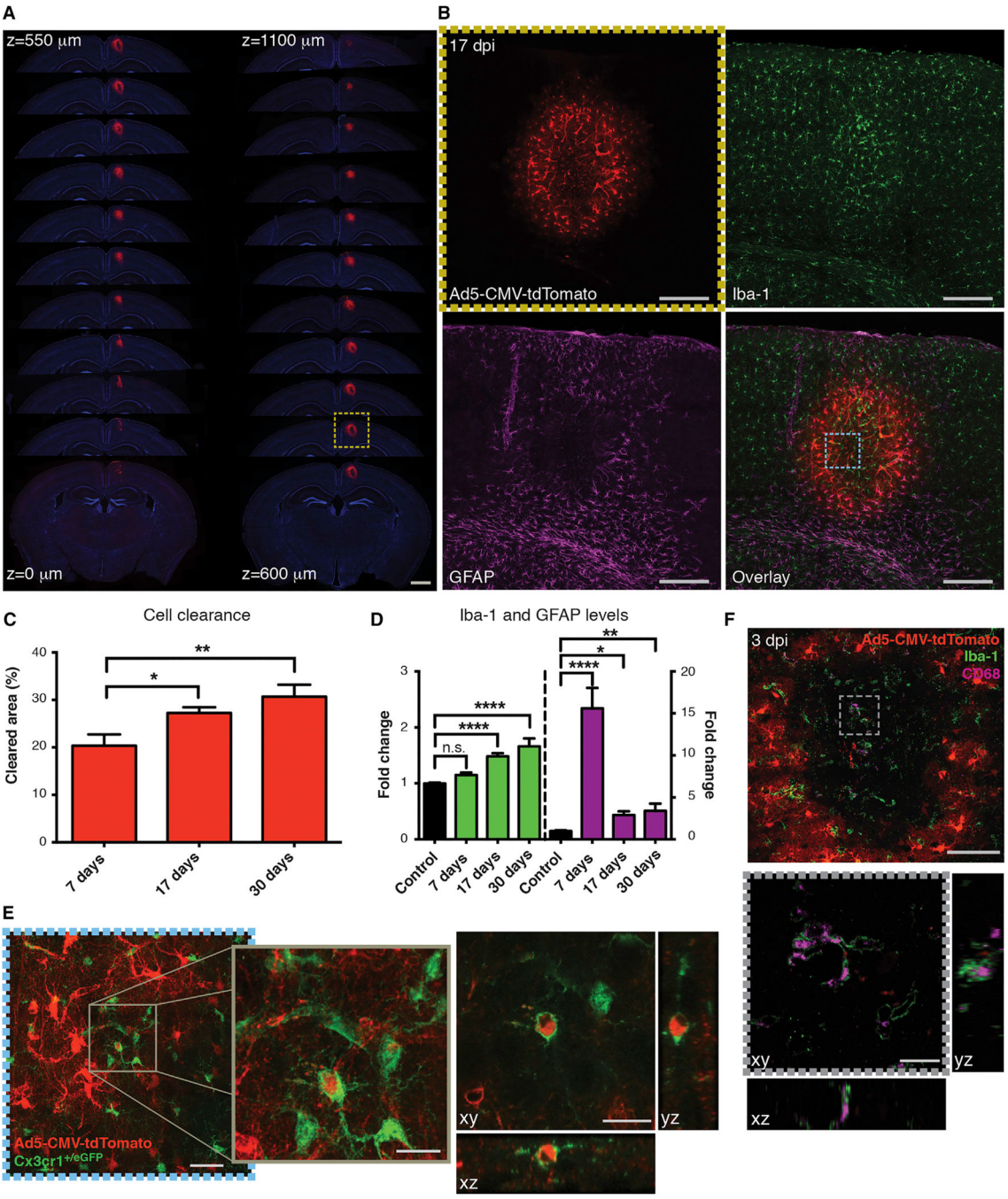

Figure 1. Microglia Engulf Adenoviral Vector-Transduced Cells

(A) Serial coronal brain sections (z) from an adult mouse 17 days after intracortical injection of 5.35×10^5 PFU of an adenovirus 5 (Ad5)-based vector that expresses tdTomato (red) under control of the CMV promoter. Sections were co-stained with DAPI (blue). Scale bar, 1 mm.

(B) tdTomato transgene expression pattern (top left), Iba-1 and glial fibrillary acidic protein (GFAP) immunoreactivity (top right and lower left), and fluorescence image overlay (lower

right) from a central brain section area, similar to the one indicated in (A) (yellow box), 17 days after intracortical vector injection. Scale bars, 200 μm.

(C) Population analysis showing that tdTomato-positive cell bodies are progressively cleared from the center toward the edges of the transduced area (see Method Details).

(D) Population data showing time-dependent Iba-1 (green) and GFAP immunoreactivity (purple) from the transduced and control hemisphere (black).

(E) Maximum-intensity projection image showing GFP-positive microglia (green) and tdTomato-positive cells in an area close to the center of the transduced area (left), similar to the area indicated in (B) (blue box). Three-dimensional image reconstruction confirms engulfment of Ad5-transduced cells by microglia (right). Scale bars, 30 μm (left) and 15 μm (center and right).

(F) Brain section showing tdTomato-positive cells (red), Iba-1-positive microglia (green), and CD68-positive lysosomes 3 days after vector injection (top). Three-dimensional image reconstruction of the indicated area (gray box) confirms the presence of CD68-positive lysosomes inside microglia. Scale bars, 50 μm (top) and 10 μm (bottom).

See also Figure S1 and Movie S1. (C) shows one-way ANOVA with Tukey's multiple comparisons test ($\alpha = 0.05$; $n \geq 5$ animals per group); (D) shows one-way ANOVA with Dunnett's multiple comparisons test ($\alpha = 0.05$; $n \geq 5$ animals per group).

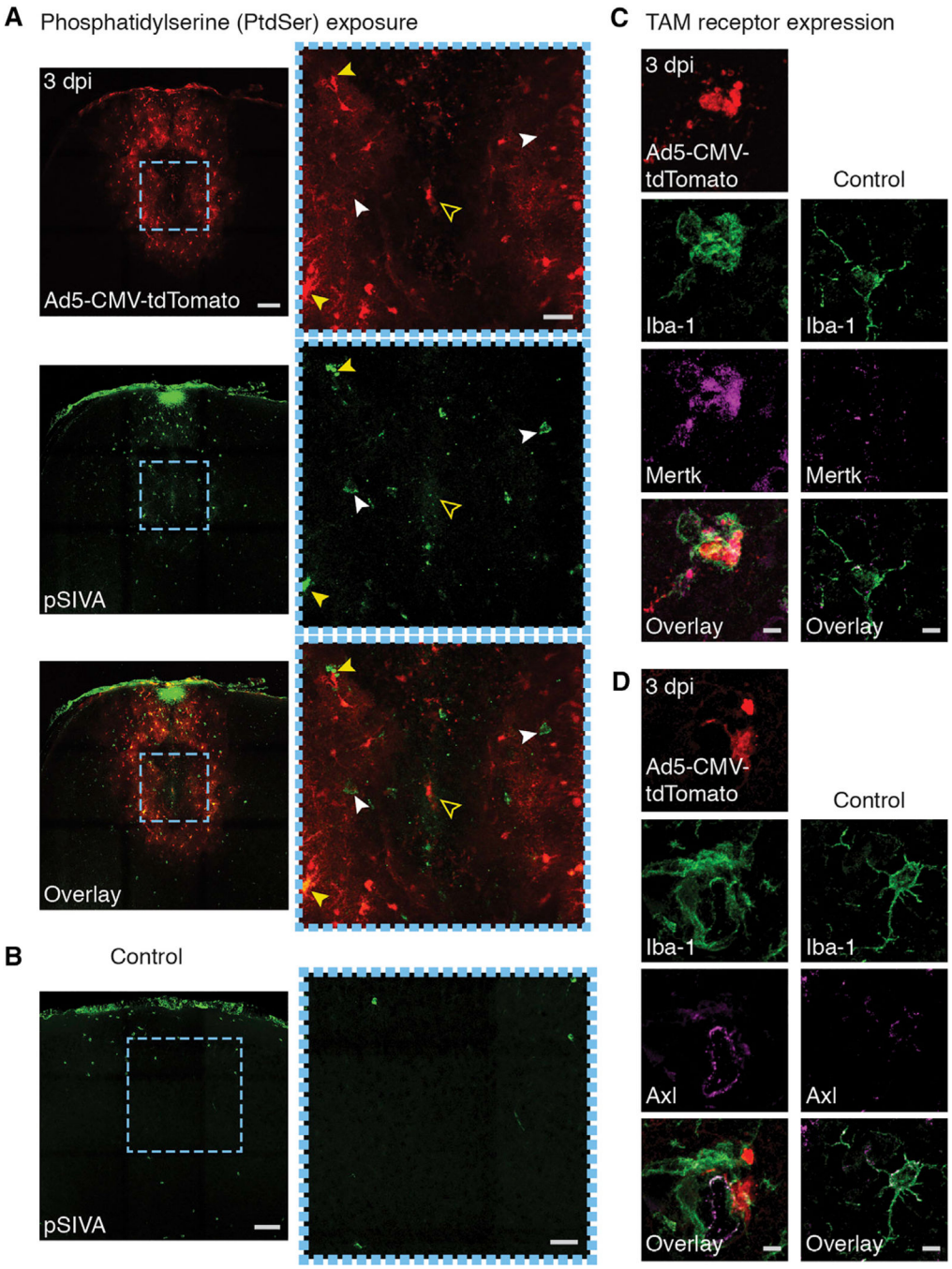

Figure 2. Adenoviral Vector Transduction Increases Phosphatidylserine Externalization and TAM Receptor Expression

(A) Fluorescence image showing transduced cells (red; top left) 3 days after intracortical Ad5 vector delivery. Phosphatidylserine on outer cell membranes was visualized using the annexin-based fluorescent indicator polarity sensitive indicator of viability and apoptosis (pSIVA) (green; center left). An image overlay is shown at the bottom. Yellow cells represent pSIVA-positive transduced cells. pSIVA staining was increased in the transduced region. Higher-magnification images of the boxed regions (blue) are shown on the right. Near central regions, pSIVA staining appears punctate, indicating cell fragmentation (open

arrowhead). In more peripheral regions, circumferential somatic membrane staining predominates indicating stressed, but live, transduced and untransduced cells (filled yellow and white arrowheads, respectively). Scale bars, 100 μm (left) and 30 μm (right).

(B) Fluorescence image showing pSIVA staining 3 days after vehicle (TMN) injection. A higher-magnification image of the boxed region (blue) is shown on the right. Scale bars, 100 μm (left) and 50 μm (right).

(C) Example immunofluorescence images showing that 3 days after vector injection *Mertk* (magenta) is upregulated on Iba-1-positive microglia (green) near central regions of the transduced area (left) compared to cells in the contralateral control hemisphere (right). Image overlays are shown at the bottom. Population data are shown in Figure 4H. Scale bars, 5 μm.

(D) Example immunofluorescence images showing that *Axl* (magenta) is also upregulated on Iba-1-positive microglia (green) near central regions (left) compared to the control hemisphere (right). Population data are shown in Figure 4H. Scale bars, 5 μm.

See also Figures S2 and S3 and Movies S2 and S3.

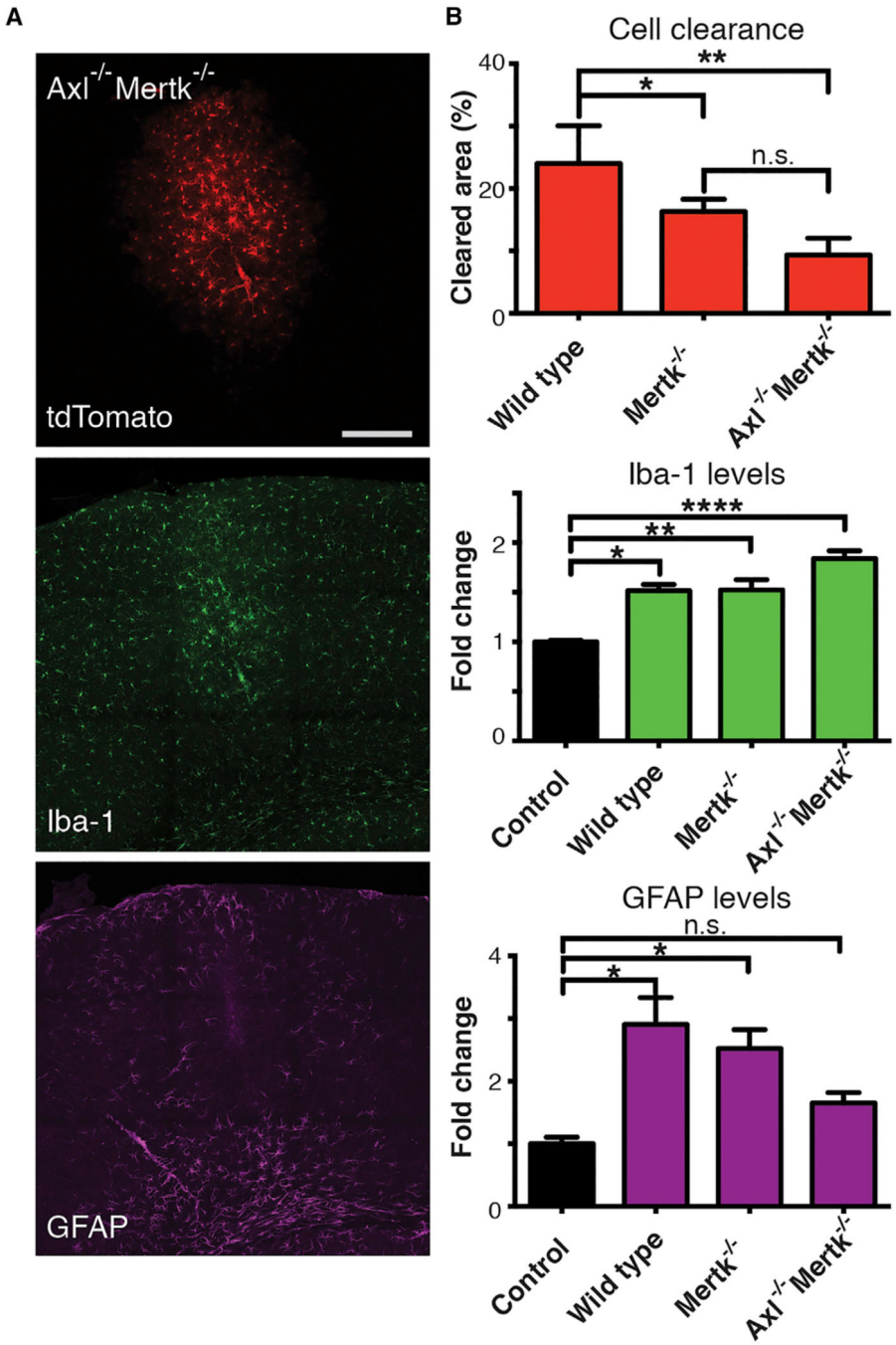

Figure 3. Microglia-Mediated Cell Clearance Depends on TAM Receptors

(A) Fluorescence images showing Ad5 CMV-promoter-driven tdTomato expression (top), Iba-1 immunoreactivity (center), and GFAP immunoreactivity (bottom) in an *Axl*$^{-/-}$ *Mertk*$^{-/-}$ double knockout mouse 17 days after vector injection. Scale bar, 200 μm.

(B) Population analysis showing cell clearance (top), Iba-1 immunoreactivity (center), and GFAP immunoreactivity (bottom) in *Mertk*$^{-/-}$ single and *Axl*$^{-/-}$ *Mertk*$^{-/-}$ double knockout mice 17 days after Ad5 injection. Contralateral hemispheres served as control regions. (B)

shows one-way ANOVA with Tukey's multiple comparisons test ($\alpha = 0.05$; $n \geq 3$ animals per group).

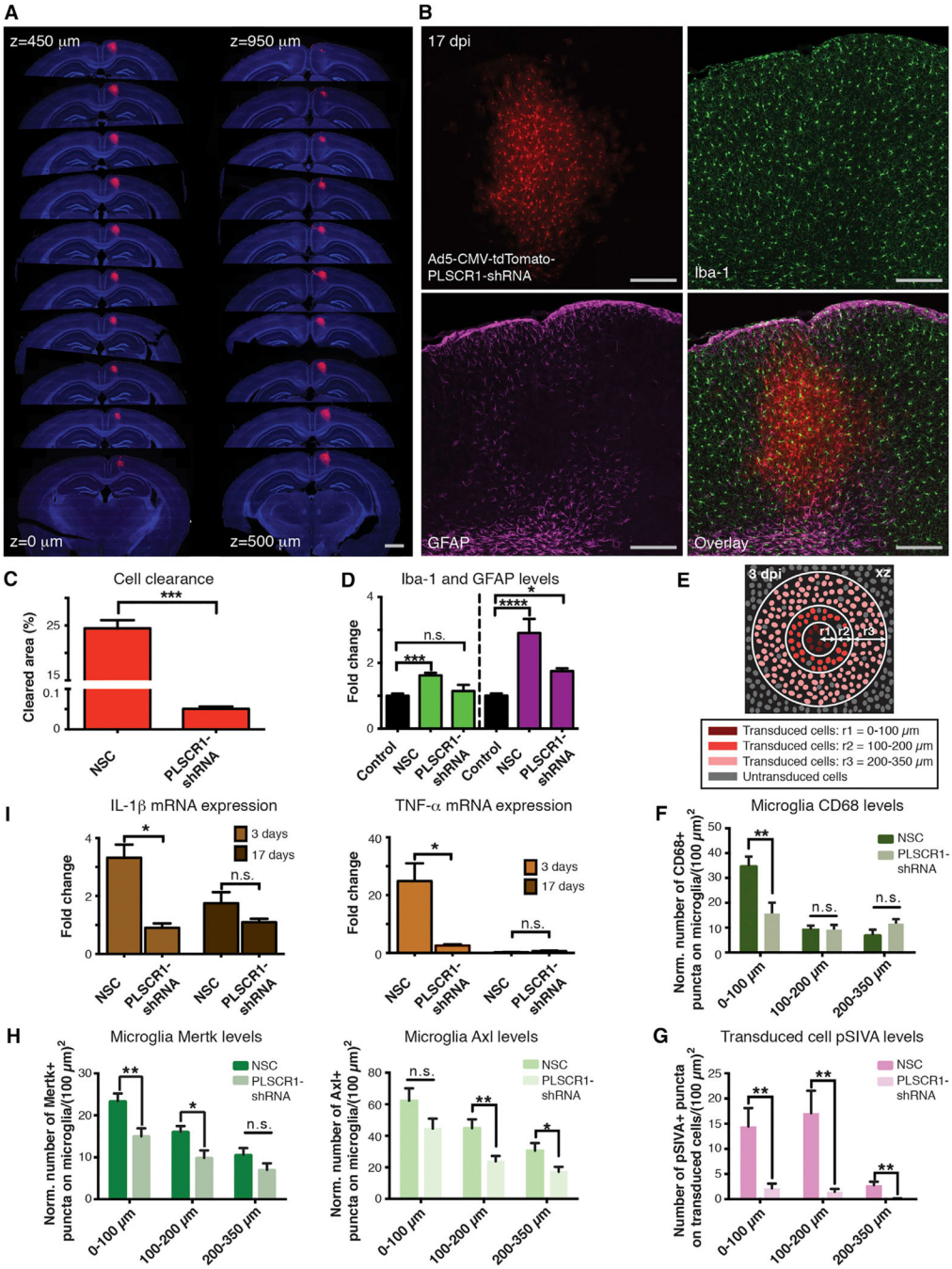

Figure 4. Phospholipid Scramblase 1 Inhibition Reduces Microglia-Mediated Cell Clearance and Cytokine Levels

(A) Serial coronal brain sections (z) from an adult mouse 17 days after intracortical injection of 5.35×10^5 PFU of an Ad5 vector that expresses tdTomato (red) and a miR30-based shRNA against mouse phospholipid scramblase 1 (PLSCR1) under control of the CMV promoter. Sections were co-stained with DAPI (blue). Scale bar, 1 mm.

(B) Transgene expression pattern (top left), Iba-1 and GFAP immunoreactivity (top right and lower left), and fluorescence image overlay (lower right) from a central brain section area 17 days after intracortical vector injection. Scale bars, 200 μm.

(C) Population analysis showing that CMV promoter-driven PLSCR1-shRNA expression can significantly reduce clearance of Ad5-transduced cells compared to a non-silencing control (NSC) shRNA at 17 days after transduction.
(D) Population data showing Iba-1 (green) and GFAP immunoreactivity (purple) for PLSCR1- and NSC-shRNA vectors. Contralateral hemispheres served as control regions (black).
(E) Schematic showing analysis regions. r denotes radial distance from the injection center.
(F) Population data showing the number of CD68-positive puncta on Iba-1-positive cells as a function of radial distance from the injection site for PLSCR1- and NSC-shRNA vectors. Data were normalized using contralateral hemispheres as control regions.
(G) Population data showing the number of pSIVA-positive puncta on tdTomato-positive transduced cells as a function of radial distance from the injection site for PLSCR1- and NSC-shRNA vectors.
(H) Population data showing the number of *Mertk*- and Iba-1-double-positive cells (left) or *Axl*- and Iba-1-double-positive cells (right) as a function of radial distance from the injection site for PLSCR1- and NSC-shRNA vectors. Data were normalized using contralateral hemispheres as control regions.
(I) qPCR population data showing PLSCR1-shRNA-mediated reduction in tissue levels of interleukin-1β (IL-1β; left) and tumor necrosis factor-α (TNF-α; right) compared to the NSC vector at 3 and 17 days after intracortical Ad5 injection. Tissue punches (see Method Details) included the transduced area and some uninfected cells in the immediate vicinity of this area.
See also Figures S4–S6. (C) shows unpaired t test (two-tailed) with Welch's correction, $p < 0.001$, $n \geq 4$ animals per group; (D) shows one-way ANOVA with Dunnett's multiple comparisons test ($\alpha = 0.05$; $n \geq 4$ animals per group); (F) shows unpaired t test ($p < 0.01$ for 0–100 μm; $n = 3$ animals per group; $N \geq 2$ slices per animal); (G) shows unpaired t test with Welch's correction ($p < 0.01$ for 0–100 μm, 100–200 μm, and 200–350 μm; $n = 3$ animals per group; $N \geq 3$ slices per animal); (H), left, shows unpaired t test ($p < 0.01$ and $p < 0.05$ for 0–100 μm and 100–200 μm, respectively; $n = 3$ animals per group; $N \geq 3$ slices per animal); (H), right, shows unpaired t test ($p < 0.01$ and $p < 0.05$ for 100–200 μm and 200–350 μm, respectively; $n \geq 2$ animals per group; $N \geq 3$ slices per animal); (I), left, shows unpaired t test (two-tailed), $p < 0.05$ ($n = 2$ animals per group); (I), right, shows unpaired t test (two-tailed), $p < 0.05$ ($n = 2$ animals per group).

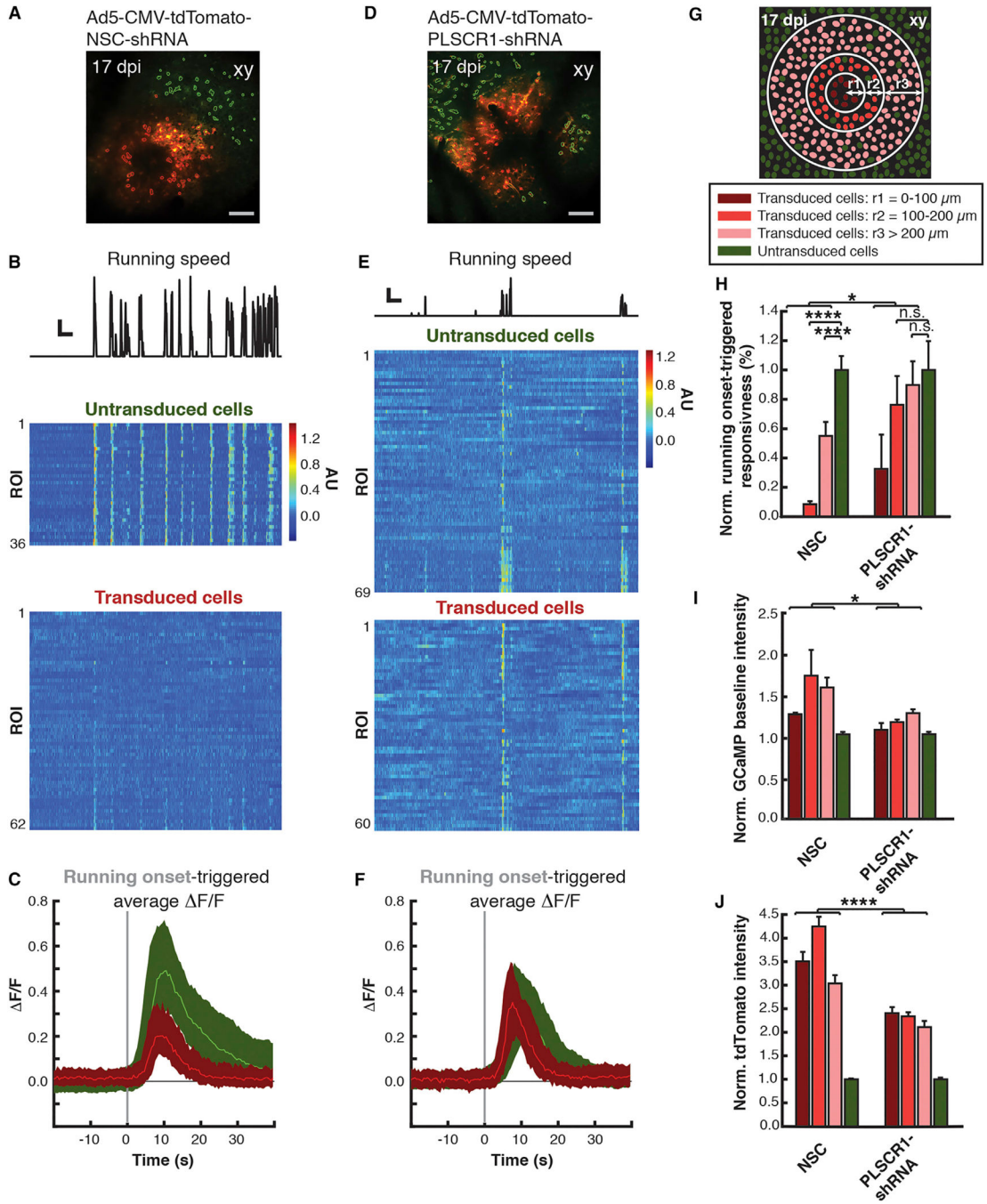

Figure 5. PLSCR1 Inhibition Reduces Intracellular Calcium Dysregulation

(A) Example two-photon fluorescence image showing Ad5-CMV-tdTomato-NSC-shRNA transduced (yellow/red) and untransduced (green) cells in the cortex of a live transgenic mouse expressing the green fluorescent, genetically encoded calcium indicator GCaMP5G under control of the GFAP promoter 17 days after intracortical vector delivery. Recordings were made at various axial depths and lateral distances from the injection site. This example recording was made at the injection site 140 μm below the pia (injection depth, 200 μm). Scale bar, 100 μm.

(B) Example calcium activity of Ad5-transduced and untransduced GCaMP5G–expressing cells in an awake, head-restrained mouse on an exercise ball. Top: mouse running speed on the ball (black). Center and bottom: corresponding ΔF/F increases in 36 untransduced and 62 transduced cells, respectively. Regions of interest (ROIs) used for analysis of calcium signals in transduced (red) and untransduced (green) cells are indicated in (A). Scale bars, 20 mm/s and 50 s.

(C) Population data showing the running onset-triggered (gray vertical line) average ΔF/F increase across Ad5-transduced (red) and untransduced (green) GCaMP5G–positive cells. The data are based on 25 (green) or 16 (red) recordings from n = 2 mice. Each recording included 2–4 running bouts.

(D) Example two-photon fluorescence image showing Ad5-CMV-tdTomato-PLSCR1-shRNA transduced and untransduced cells in the cortex of a live transgenic mouse expressing GCaMP5G under control of the GFAP promoter 17 days after intracortical vector delivery (recording depth, 120 μm). Elongated dark regions are due to light absorption by surface blood vessels. Scale bar, 100 μm.

(E) Example calcium activity of Ad5-transduced and untransduced GCaMP5G–positive cells in an awake, head-restrained mouse on an exercise ball. Top: mouse running speed on the ball (black). Center and bottom: corresponding ΔF/F increases in 69 untransduced and 60 transduced cells, respectively. ROIs used for analysis of transduced (red) and untransduced (green) cells' calcium signals are indicated in (D). Scale bars, 20 mm/s and 50 s. Note the difference in transduced cells' responsiveness to running onset compared to (B).

(F) Population data showing the running onset-triggered (gray vertical line) average ΔF/F increase across Ad5-transduced (red) and untransduced (green) GCaMP5G–positive cells. The data are based on 20 (green) or 12 (red) recordings from n = 3 mice. Each recording included 2–4 running bouts.

(G) Schematic showing analysis regions. r denotes radial distance from the injection center.

(H–J) Population data showing running onset-triggered responsiveness (H), GCaMP5G baseline fluorescence (I), and tdTomato fluorescence (J), respectively, of Ad5-CMV-tdTomato-NSC-shRNA (left, red bars) or Ad5-CMV-tdTomato-PLSCR1-shRNA transduced cells (right, red bars) as a function of radial distance from the center of the injection site. Data were normalized to untransduced cells far away from the injection site (green; Figures S7H–S7J).

See also Figure S7. Shaded areas in (C) and (F) represent the 75% and 25% percentile of the mean; (H) shows paired t test (Bonferroni corrected) for comparisons within the NSC ($p < 0.0001$) or PLSCR1-shRNA group and unpaired t test (Bonferroni corrected) for comparison between the two groups ($p < 0.05$); (I) and (J) show unpaired t test (Bonferroni corrected; $p < 0.05$ and $p < 0.0001$, respectively); the NSC or PLSCR1-shRNA group data in (H)–(J) are based on 25 recordings from n = 2 mice (1,208 untransduced cells and 48, 337, 183 transduced cells within 0–100 μm, 100–200 μm, and >200 μm, respectively) or 20 recordings from n = 3 mice, respectively (1,398 untransduced cells and 130, 363, 290 transduced cells within 0–100 μm, 100–200 μm, and >200 μm, respectively). Each recording included 2–4 running bouts.

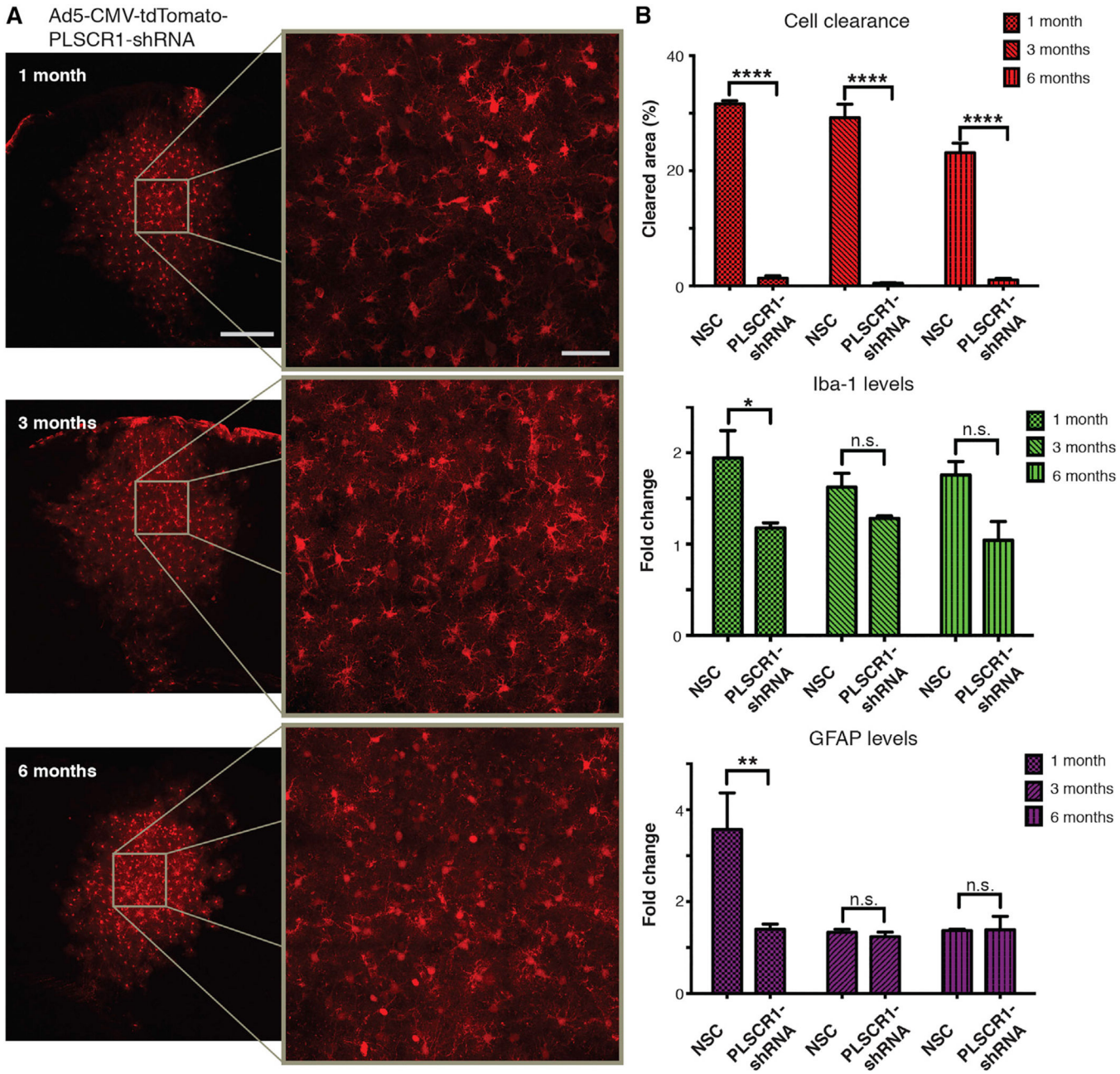

Figure 6. PLSCR1 Inhibition Provides Long-Term Protection from Microglia-Mediated Cell Clearance

(A) Fluorescence images showing Ad5-transduced tdTomato- and PLSCR1-shRNA-expressing cells 1 month (top), 3 months (center), and 6 months (bottom) after intracortical vector injection in three different mice. Close ups show morphology of transduced cells near central regions of the transduced area. Scale bars, 200 μm (left) and 50 μm (right).

(B) Population data showing cell clearance (top), Iba-1 immunoreactivity (center), and GFAP immunoreactivity (bottom) at 1 month, 3 months, or 6 months after intracortical injection of Ad5 with PLSCR1- or NSC-shRNA. (B) shows two-way ANOVA with Sidak's multiple comparisons test ($\alpha = 0.05$; $n \geq 3$ animals per group).

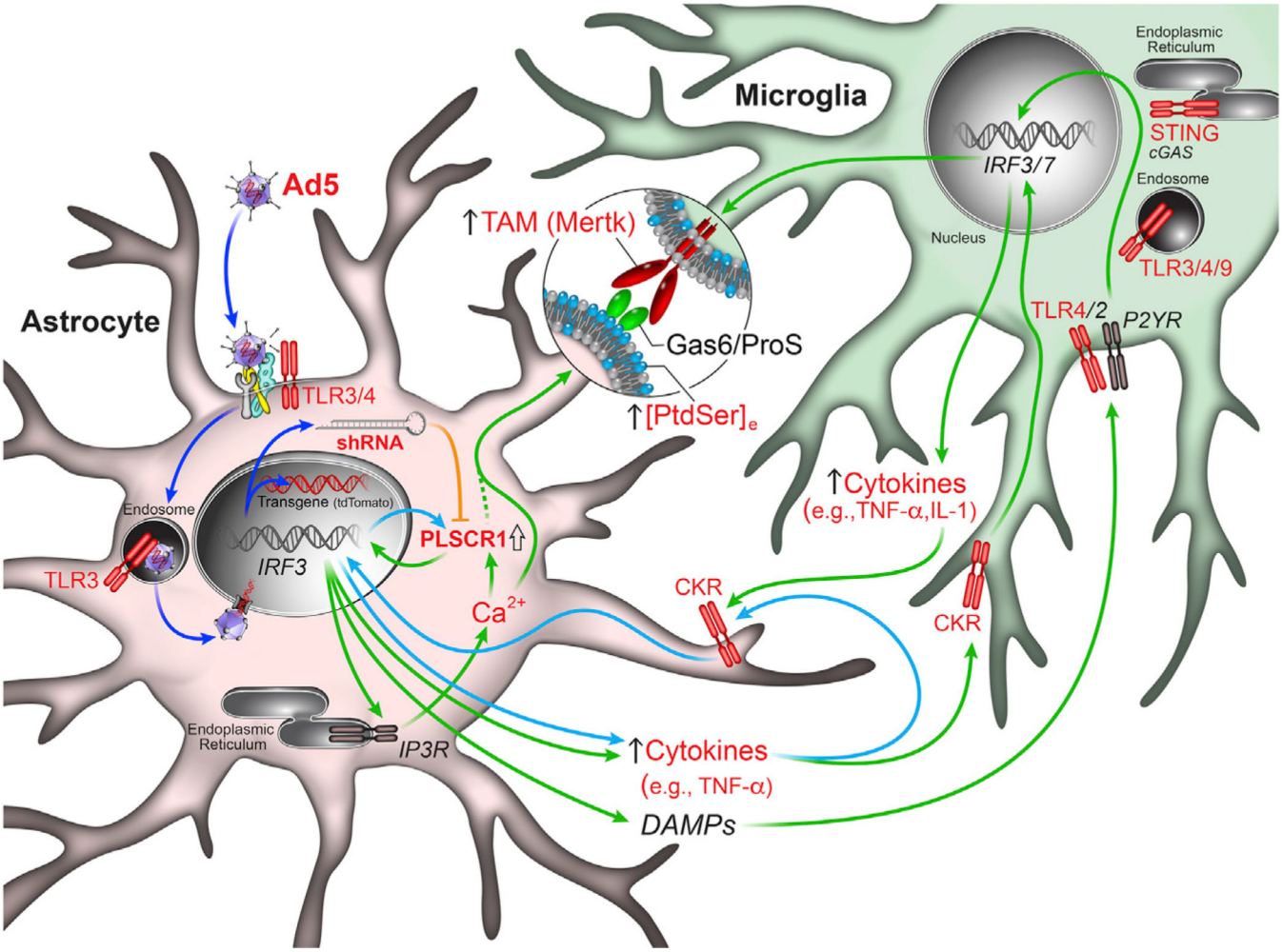

Figure 7. Model of Signaling Pathways Involved in Microglia Phagocytosis of Adenoviral Vector-Transduced Cells

Ad5 enters cells with appropriate surface receptors, particularly astrocytes. During entry or intracellular trafficking, Ad5 is sensed, a process that likely involves Toll-like receptor (TLR) signaling (Figure S2). This results in an initial burst of pro-inflammatory cytokines and phospholipid scramblase 1 (PLSCR1) activity modulation. PLSCR1, in turn, induces changes in intracellular calcium (Ca^{2+}) signaling, including blunted Ca^{2+} transients and increased calcium baseline (Figure 5). Dysregulation of intracellular Ca^{2+} homeostasis promotes phosphatidylserine (PtdSer) externalization either directly or indirectly. Additionally, it may lead to the release of damage-associated molecular patterns (DAMPs). Chemotactic gradients established by stressed cells attract microglia to central transduced regions (Movie S2). TAM receptor-mediated recognition of PtdSer-tagged cells triggers microglia phagocytosis. Engulfment of transduced cells facilitates detection of cellular DNA by microglial TLRs or STING, stimulating the production of secondary cytokines, thereby promoting cell death and bystander damage (Figure 2A; Figure S1E). shRNA-mediated knockdown of PLSCR1 (yellow) reduces dysregulation of intracellular Ca^{2+} homeostasis, PtdSer externalization, and, potentially, DAMP release. This, in turn, lowers TAM receptor-mediated detection of stressed cells, their phagocytosis, and secondary cytokine production.

A similarly protective effect can be achieved by expression of calcium-insensitive, mutant $PLSCR1_{D284A}$ (Figure S6). PLSCR1 modulation can therefore act as a potent inhibitor of innate immune responses to Ad5-based vectors, enabling long-term expression of desired transgene(s). Blue and green arrows indicate likely events upstream of PLSCR1 activation and pathways affected by PLSCR1 modulation, respectively. Red indicates molecular players/mechanisms investigated in this study. Putative pathways/mechanisms are italicized. See text for more details. Abbreviations: CKR, cytokine receptor; cGAS, cyclic GMP-AMP synthase; Gas6, growth arrest-specific 6; IP3R, inositol 1,4,5-triphosphate receptor; IRF3/7, interferon regulatory factor 3/7; ProS, protein S; P2YR, P2Y purinoreceptor; STING, stimulator of interferon genes.

KEY RESOURCES TABLE

REAGENT or RESOURCE	SOURCE	IDENTIFIER
Antibodies		
Mouse monoclonal anti-GFAP (clone GA5)	EMD Millipore	Cat#MAB3402; RRID: AB_94844
Rabbit polyclonal anti-NeuN	EMD Millipore	Cat#ABN78; RRID: AB_10807945
Rabbit polyclonal anti-Iba1	Wako	Cat#019-19741; RRID: AB_839504
Rat monoclonal anti-CD68 (clone FA-11)	Bio-Rad	Cat#MCA1957; RRID: AB_322219
Goat polyclonal anti-Axl	R&D Systems	Cat#AF854; RRID: AB_355663
Goat polyclonal anti-Mer	R&D Systems	Cat#AF591; RRID: AB_2098565
Rat monoclonal anti-Mer	eBioscience	Cat#14-5751; RRID: AB_2572885
Goat anti-rabbit IgG (H+L) secondary antibody, Alexa Fluor 488	Thermo Fisher Scientific	Cat#A-11034; RRID: AB_2576217
Goat anti-mouse IgG (H+L) secondary antibody, Alexa Fluor 633	Thermo Fisher Scientific	Cat#A-21052; RRID: AB_2535719
Goat anti-rat IgG (H+L) secondary antibody, Alexa Fluor 633	Thermo Fisher Scientific	Cat#A-21094; RRID: AB_2535749
Goat anti-rabbit IgG (H+L) secondary antibody, HRP	Thermo Fisher Scientific	Cat#31460; RRID: AB_228341
Rabbit polyclonal anti-adenovirus type 5	Abcam	Cat#ab6982; RRID: AB_305685
Chemicals, Peptides, and Recombinant Proteins		
pSIVA-IANBD	Novus Biologicals	Cat#NBP2-29382
Target retrieval solution	Dako	Cat#S170084-2
EGF recombinant human protein	GIBCO	Cat#PHG0314
DAPI, FluoroPure grade	Thermo Fisher Scientific	Cat#D21490
PNPP (p-nitrophenyl phosphate)	Thermo Fisher Scientific	Cat#34047
Diethanolamine substrate buffer	Thermo Fisher Scientific	Cat#34064
Critical Commercial Assays		
RNeasy mini kit	QIAGEN	Cat#74104
RNeasy midi kit	QIAGEN	Cat#75142
Transcriptor first strand cDNA synthesis kit	Roche	Cat#04379012001
SYBR green PCR master mix	Thermo Fisher Scientific	Cat#4344463

REAGENT or RESOURCE	SOURCE	IDENTIFIER
Experimental Models: Cell Lines		
Cell line: 293-H	O'Shea and Powers, 2013	N/A
Cell line: 293e4/ix	O'Shea and Powers, 2013	N/A
Experimental Models: Organisms/Strains		
Mouse: Cx3cr1$^{+/eGFP}$: B6.129P–Cx3cr1^{tm1Litt}/J	The Jackson Laboratory	RRID: IMSR_JAX:005582
Mouse: S100b–eGFP: B6;D2-Tg(S100B-EGFP)1Wjt/J	The Jackson Laboratory	RRID: IMSR_JAX:005621
Mouse: Gfap-Cre (73.12): B6.Cg-Tg(Gfap-cre)73.12Mvs/J	The Jackson Laboratory	RRID: IMSR_JAX:012886
Mouse: CAG-GCaMP5G–IRES-tdTomato: B6;129S6-Polr2a$^{tm1(CAG-GCaMP5g,-tdTomato)Tvrd}$/J	The Jackson Laboratory	RRID: IMSR_JAX:024477
Mouse: Mertk$^{-/-}$: B6;129-Mertk^{tm1Grl}/J	The Jackson Laboratory	RRID: IMSR_JAX:011122
Mouse: Axl$^{-/-}$: STOCK Axl^{tm1Grl}/J	The Jackson Laboratory	RRID: IMSR_JAX:011121
Mouse: TLR3$^{-/-}$: B6N.129S1-Tlr3^{tm1Flv}/J	The Jackson Laboratory	RRID: IMSR_JAX:009675
Mouse: TLR4$^{-/-}$: B6.B10ScN-Tlr4$^{lps-del}$/JthJ	The Jackson Laboratory	RRID: IMSR_JAX:007227
Mouse: TLR9$^{-/-}$: C57BL/6J–Tlr9^{M7Btlr}/Mmjax	Mutant Mouse Resource & Research Centers	RRID: MMRRC_034329-JAX
Mouse: STING$^{-/-}$: C57BL/6J–Tmem173^{gt}/J	The Jackson Laboratory	RRID: IMSR_JAX:017537
Mouse: IFNAR1$^{-/-}$: B6.129S2-Ifnar1^{tm1Agt}/Mmjax	Mutant Mouse Resource & Research Centers	RRID: MMRRC_032045-JAX
Mouse: IL-1R1$^{-/-}$: B6;129S1-Il1r1^{tm1Roml}/J	The Jackson Laboratory	RRID: IMSR_JAX:003018
Mouse: TNF$^{-/-}$: B6.129S–Tnf^{tm1Gkl}/J	The Jackson Laboratory	RRID: IMSR_JAX:005540
Recombinant DNA		
Adenovirus: Ad5-CMV-tdTomato-NSC-shRNA Titer (PFU/ml): 2.97×10^{10} Particle-to-PFU ratio: 11	This paper	N/A
Adenovirus: Ad5-CMV-tdTomato-PLSCR1-shRNA Titer (PFU/ml): 6.16×10^{9} Particle-to-PFU ratio: 22	This paper	N/A
Adenovirus: Ad5-CMV-PLSCR1$_{D284A}$-P2A-tdTomato Titer (PFU/ml): 2.12×10^{8} Particle-to-PFU ratio: 577	This paper	N/A
Adenovirus: Ad5-CMV-Null Titer (PFU/ml): 4.88×10^{10} Particle-to-PFU ratio: 24	This paper	N/A

REAGENT or RESOURCE	SOURCE	IDENTIFIER
Adenovirus: Human adenovirus 5	ATCC	Cat#VR-1516
Plasmid: AdSyn Ad5 module pCOE1-038	O'Shea and Powers, 2013	N/A
Plasmid: AdSyn Ad5 module pCOASMM-025	O'Shea and Powers, 2013	N/A
Plasmid: pUNISHER	Montesinos et al., 2011	N/A
Plasmid: pGIPZ shRNA miR control vector	GE Dharmacon	Cat#RHS4346
Plasmid: pCMV6-mPLSCR1-myc-DDK	OriGene	Cat#MR204796
Sequence-Based Reagents		
Primer: TNF-α Fwd: GCCACCACGCTCTTCTGTCT Rev: CAGCTGCTCCTCCACTTGGT	This paper	N/A
Primer: IL-1β Fwd: CCTCTCCAGCCAAGCTTCC Rev: CTCATCAGGACAGCCCAGGT	This paper	N/A
Primer: mPLSCR1–3 Fwd: GCGCAGCTAGAGGATTCAGG Rev: AACAGTTTCTGAGGCTCCTTCT	This paper	N/A
Primer: 36B4 Fwd: CTCTCGCTTTCTGGAGGGTG Rev: ACGCGCTTGTACCCATTGAT	This paper	N/A
Primer: Cyclophilin A Fwd: GCCGATGACGAGCCCTT Rev: AAGTCACCACCCTGGCACA	This paper	N/A
Software and Algorithms		
MATLAB, Version 15b	MathWorks	https://www.mathworks.com/products/matlab.html
Imaris, Version 7 and 8	Bitplane	http://www.bitplane.com/imaris
Fiji	SciJava	https://fiji.sc
GraphPad Prism, Version 7	GraphPad Software	http://www.graphpad.com/scientific-software/prism/
Applied Biosystems qPCR analysis modules (cloud-based), Version 2.0	Thermo Fisher Scientific	https://www.thermofisher.com/us/en/home/cloud/all-analysis-modules/ab-secondary-data-analysis-modules.html

Neuron. Author manuscript; available in PMC 2018 February 08.